Biointerface Research in Applied Chemistry
Open-Access Journal (ISSN: 2069-5837)

Article
Volume 13, Issue 3, 2023, 202
https://doi.org/10.33263/BRIAC133.202

Manifestation of Intermolecular Interactions in the IR Spectra of 2- and 4-Methylmethcathinones Hydrochlorides: DFT Study and Hirshfeld Surfaces Analysis

Valentina Minaeva [1], Alexandr Panchenko [1], Nataliya Karaush-Karmazin [1,*], Jacek E. Nycz [2], Boris Minaev [1]

[1] Department of Chemistry and Nanomaterials Science, Bohdan Khmelnytsky National University, 18031 Cherkasy, Ukraine
[2] Institute of Chemistry, Faculty of Science and Technology, University of Silesia in Katowice, ul. Szkolna 9; PL-40007 Katowice, Poland
* Correspondence: karaush22@ukr.net (N.K.-K.);

Scopus Author ID 56031425800
Received: 11.03.2022; Accepted: 13.04.2022; Published: 31.05.2022

Abstract: This paper reports a Hirshfeld surfaces analysis of crystalline 2- and 4-methylmethcathinone (2-MMC and 4-MMC) hydrochlorides to analyze NH·Cl and CH···Cl intermolecular interactions and approve the formation of the NH_2^+–Cl^- salt fragment in both 2-MMC·HCl and 4-MMC·HCl crystals. Two isomeric dimers were separated from the corresponding crystal packing to model IR spectra of the crystalline 2-MMC·HCl and 4-MMC·HCl species within the framework of density functional theory (DFT) and B3LYP/6-31G(d,p) approach. All observed IR bands were assigned and interpreted in the experimental spectra of the 2-MMC·HCl and 4-MMC·HCl standard crystal samples representing an important aspect of the forensic problem solvation. A detailed analysis of the nature of IR spectra for both isomers has shown that intermolecular interactions between the NH_2^+ and Cl^- ionic moieties occur in two crystalline samples. The presence of the ionized form of the 2- and 4-MMC·HCl compounds with the $NH_2^+Cl^-$ fragment is a key condition for the correct reproduction of the IR spectra when calculating the corresponding dimer structures as a model of a crystalline sample.

Keywords: 2-methylmethcathinone hydrochloride; 4-methylmethcathinone hydrochloride; IR spectrum; Hirshfeld surfaces analysis; DFT calculations; Bader's QTAIM analysis.

1. Introduction

Cathinone (2-amino-1-phenyl propanone) is an alkaloid responsible for khat intoxication [1,2]. This class of compounds can be considered *β*-keto analogs of amphetamine (1-phenylpropan-2-amine) because of its almost identical structure (Figure 1) [3]. The molecular skeleton of cathinone represents a polyfunctional backbone that can be easily modified in several predictable manipulations, including aromatic ring substitution, *N*-alkylation, or/and variation of the alkyl substituents in the structure of cathinone (Figure 1). Such simple structural manipulations lead to new designer cathinone derivatives with similar stimulant effects and represent an active research area [4–10]. Several cathinones such as amfepramone [11,12], bupropion [13,14], and pyrovalerone [15,16] are used in pharmacology.

However, most of the newly synthesized cathinones are gaining popularity as a legal alternative to illicit drugs of abuse.

By the end of 2021, 830 new psychoactive substances (NPS) were monitored by European Monitoring Centre for Drugs and Drug Addiction (EMCDDA). Among them, there are 209 cannabinoids and 156 cathinone. Totally 46 NPS were first reported in 2020. Since 2015, about four hundred previously unreported NPS appeared on the European market each year. Therefore, the development of the analytical method is of great importance for forensic medical examination in cases of drug trafficking [17–21]. X-ray diffraction, NMR, and vibrational spectroscopy are generally used for structure determination and finger printing, *i.e.*, identifying unknown compounds [22]. The electrophoretic (capillary electrophoresis) and chromatographic (gas and liquid chromatography) techniques are the most important tools for the separation of chiral drugs on an analytical scale, *i.e.*, for analysis of their enantiomeric purity [23–26]. Gas chromatography-mass spectrometry (GC–MS) provides a reliable analysis platform commonly used in forensic chemistry to identify controlled substances [27]. In this respect, quantum chemical calculations can efficiently predict the structure and spectra of newly synthesized and insufficiently experimentally characterized cathinone [28–32].

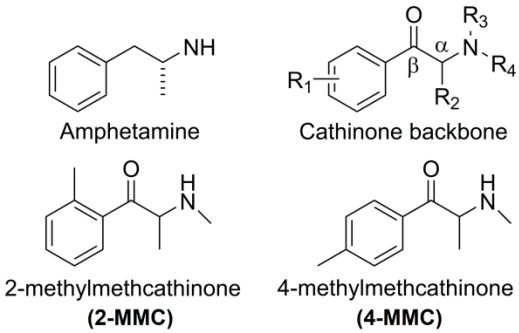

Figure 1. The structure of amphetamine, 2-methylmethcathinone and 4-methylmethcathinone. The cathinone backbone is given along with four regions where functionalization is possible.

In our recent density functional theory (DFT) study of 1-(4-chlorophenyl)-2-(ethylamino)propan-1-one (4-chloroethylcathinone or 4-CEC) hydrochloride, it was proven that the presence of the $NH_2^+Cl^-$ fragment in the ionized form of the 4-CEC is a key condition for the correct reproduction of the IR spectrum of a crystalline 4-CEC sample [33]. Since the *N*-methyl derivatives or methcathinone were the most commonly abused synthetic drugs [34], a further quantum chemical computational analysis of the electronic descriptors should be performed. Analytical, chemical, and pharmaceutical data of methcathinone including 2-(methylamino)-1-(4-methylphenyl)propan-1-one or 4-methylmethcatinone and it's 2- and 3-methyl methcathinone isomers were reported in Refs. [35–41].

The most popular and accessible drug mephedrone (4-methylmethcathinone, 4-MMC) is synthesized in the form of free base cathinone (4-MMC) and the form of more stable salt compound 4-methyl methcathinone hydrochloride (4-MMC·HCl). The experimental IR spectrum of 4-MMC (vapor phase) and 4-MMC·HCl (crystals of the salt) have been detected in Ref. [36], but without assignment of the bands' origin. Power et al. [37] have presented IR spectra of three synthesized 2-, 3- and 4-isomers of methyl methcathinone hydrochlorides and have shown that these spectra can be used to discern these three compounds with analytical accuracy. In Refs. [36,37,40,41], however, not much attention has been paid to the analysis of the high-frequency IR region, where valence stretching N–H···Cl and C–H···Cl are revealed, and assignments of some IR bands are doubtful.

In a recent study [42], the quantum-chemical calculations of IR, UV, and NMR spectral properties based on the density functional theory [43] are presented. Starting from the initial molecular geometries obtained by the PM3 approach [44,45], we have predicted the DFT-optimized structure of the 4-MMC isomer as the gas-phase molecule by complete calculation of its force field the corresponding global minimum on the potential energy surface in the multidimensional space of all internal variables. On such backgrounds, we have simulated and assigned all vibrational modes in the IR spectrum of the 4-MMC molecule. This psychotropic substance's DFT calculated IR spectrum really does contain all absorption bands corresponding to frequencies and relative intensities of the measured experimental vapor-phase IR spectrum of the 4-MMC isomer being the synthesized standard sample [36]. However, starting from initial molecular geometries generated by the PM3 method [44,45] for the salt structure of 4-MMC·HCl cathinone, the DFT approach comes to HCl coordination with the oxygen atom of the carbonyl group of methcathinone, which does not correspond to the X-ray diffraction data, obtained in the study of Nycz et al. [40]. These authors [40] (besides the X-ray diffraction data) have also studied the FTIR absorption spectrum of 4-MMC salt powder. However, they have assigned only a few simplest characteristic bands in their FTIR spectrum.

Here we represent a detailed interpretation of the IR spectra of 2- and 4-methyl methcathinone (shortly named 2-MMC and 4-MMC) hydrochloride crystalline samples with the DFT method taking into account X-ray data. Crystal structures of 2-MMC·HCl and 4-MMC·HCl are available in Refs. [40,41]. The Hirshfeld surfaces analysis of crystalline 2-MMC and 4-MMC hydrochlorides is performed here to analyze the intermolecular interactions and correctly select the corresponding dimer structures as models for the reproduction of the experimental IR spectra by the DFT method.

2. Materials and Methods

2.1. Computational details.

The Hirshfeld surface analysis (HSA) of the studied 2-and 4-MMC crystals and their corresponding 2D fingerprint plots were performed using the Crystal Explorer 21.5 software at a very high resolution [46]. The HSA represents a simple and aesthetically pleasing approach for the identification and representation of all close atomic contacts in crystals.

According to HSA, the molecular density at each point *r* among the atoms of the molecule (promolecule density) is written as [47,48]

$$\rho^{pro}(r) = \sum_i \rho_i^{at}(r), \quad (1)$$

where the individual $\rho_i^{at}(r)$ is spherically averaged ground-state atomic densities.

A sharing function for each atom in a molecule is defined as

$$w_a(r) = \rho_a^{at}(r)/\rho^{\text{promol}}(r). \quad (2)$$

In this context, the electron density of an atomic fragment produces the following relation

$$\rho_a(r) = w_a(r)\rho^{\text{mol}}(r), \quad (3)$$

where $\rho^{\text{mol}}(r)$ represents the molecular electron density.

A weight function of a molecule in a crystal can be written as

$$w_A(r) = \rho^{promol}(r)/\rho^{\text{procrystal}}(r). \quad (4)$$

The Hirshfeld surface (Figure 2) is visualized by the normalized contact distance (d_{norm}), which is defined in terms of external and internal distances (d_e and d_i, respectively), and the van der Waals radii (*vdW*) of atoms is computed with the following equation [46–48]:

$$d_{norm} = \frac{d_i - r_i^{vdW}}{r_i^{vdW}} + \frac{d_e - r_e^{vdW}}{r_e^{vdW}}, \quad (5)$$

where r_i^{vdW} and r_e^{vdW} are the van der Waals radii of the appropriate atoms internal and external to the surface, respectively. The contacts with distances equal to the sum of the *vdW* radii are indicated in white in Figure 2, and the contacts with distances shorter or longer than *vdW* radii are represented in red and blue, respectively.

To simulate intermolecular interactions in the crystal, the quantum chemical DFT [49,50] calculations were carried out for the dimers isolated from the 2- and 4-MMC crystal structures. The structures of the studied dimers were optimized at the B3LYP/6–31G(d,p) [43,51,52] level of theory using the Gaussian 16 package [53]. Vibrational frequencies and the corresponding IR intensities were calculated for the optimized geometry of the 2- and 4-MMC·HCldimers at the same computational level.

To compare the calculated spectrum with the experimental IR spectrum of compounds 2-MMC and 4-MMC, the calculated vibrational frequencies were scaled with different scale factors for two optical regions: 0.945 for high-frequency valence vibrations and 0.97 for the 1700–500 cm^{-1} spectral region. The scale factors were estimated as the averaged ratio between the experimentally observed and DFT-calculated frequency of all bands in a particular IR region. We should note that similar values of the scaling factors were obtained before and are typical for many organic molecules in the corresponding spectral regions [54–58]. The calculated IR spectra of the 2- and 4-MMC·HCl dimers were constructed using the SWizard 4.6 program [59] (with the Lorentzian distribution function). The detailed assignment of all fundamental modes in the IR spectra was obtained from the calculated vibrational animation with the GaussView 6.0 program [60], which visualizes vibrational movements.

Non-covalent interaction parameters for the 2- and 4-MMC·HCl dimers were calculated within the framework of the Bader method "Quantum Theory of Atoms In Molecules" (QTAIM) [61] using the AIMAll software [62]. The energies of non-covalent bonds (*E*) were estimated by the Espinosa-Molins-Lecomte (EML) equation [58–65]:

$$E = 0.5\, v(r), \quad (6)$$

where $v(r)$ is the potential energy density value in the corresponding (3, -1) bond critical point [61].

3. Results and Discussion

3.1. Hirshfeld surface (HS) analysis.

To gain insight into the nature of the intermolecular contacts stabilizing the crystal structures of the 2- and 4-MMC·HCl and to explain the peculiarities of the influence of these intermolecular interactions on their IR spectra, the HS analysis was carried out. The hydrochloride salts of 2-MMC and 4-MMC crystallize in the orthorhombic (*Pbca*) and monoclinic ($P2_1/n$) space groups [40,41], respectively. The cell packing and HS of the 2- and 4-MMC·HCl are presented in Figure 2. It includes several dimers; one has to stress also different types of the N–H–Cl interactions of the N-H group with its counter anion and those

links with another Cl anion from the neighboring molecule (the second cation partner in the dimer). The late intermolecular link is denoted as N–H···Cl bonding.

As one can see in the Hirshfeld d_{norm} surface plot for both 2- and 4-MMC (*i.e.*, 2- or 4-MMC cation and chlorine ion), the N–H···Cl interactions between the chlorine ion and the hydrogen atom of the amino group of the neighboring cation represent the most prominent intermolecular contacts with distances of 2.466 and 2.226 Å in 2- and 4-MMC crystals, respectively, and are indicated as dark red spots in HS. The shortest contacts 2.272 and 2.182 Å in crystals of 2- and 4-MMC, respectively, can be considered as N–H–Cl intramolecular interactions between the hydrogen atom of the amino group of 2-MMC/4-MMC cation connected directly with its native chloride ion; therefore, these contacts are not indicated by the red spot on the HS. The other contacts 2.920 and 2.591 Å in 2-MMC crystal and 2.643 and 2.867 Å in 4-MMC crystal, correspond to the CH···Cl link contacts.

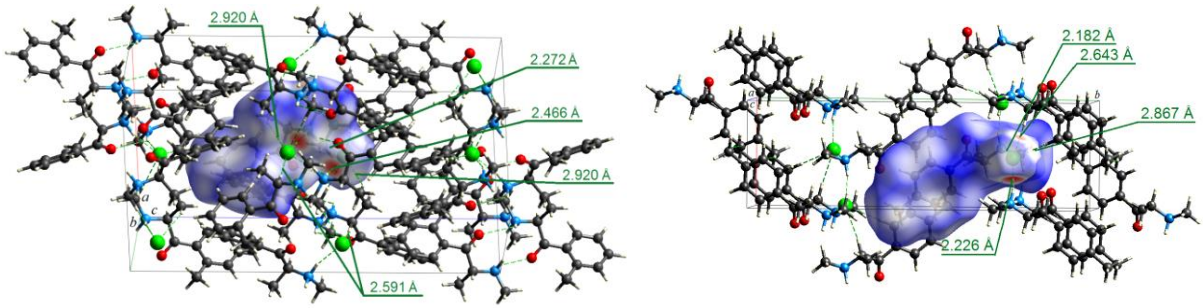

a *b*

Figure 2. Hirshfeld d_{norm} surface of the intermolecular interactions for 2-MMC (*a*) and 4-MMC (*b*); green Cl, blue N, red O, grey C atoms.

Figure 3 shows a 2D fingerprint plot detailing the percentage at which each meaningful contact occurs, including an overall plot of all contacts. For both 2-MMC and 4-MMC, the H···H interactions appear as the largest region (55.1 and 53.7 %, respectively) of the fingerprint plot with a high concentration at $d_e = d_i \sim 1.2$ Å. The Cl···H interactions in the fingerprint plot are pictured by the two distinct spikes of equal lengths. The contribution to the total surface area for Cl···H contacts is 19.4% for 2-MMC and 21.0% for 4-MMC. The C···H contacts contribute 16.2% when the methyl group is at *meta* position on the phenyl ring (2-MMC) and 13.7% in the case of *para*-substituted phenyl ring (4-MMC) and show the two pairs of characteristic wings in the fingerprint plot (Figure 3). In addition, the O· ·H contacts are present in the wide central part of the HS with contributions of 8.9 and 11.0% for 2- and 4-MMC, respectively. The contribution of the C···C contacts, responsible for the π-π stacking interactions, reaches only 1%. This indicates that the supramolecular arrangement in both crystals is mainly due to the hydrogen bonds discussed above.

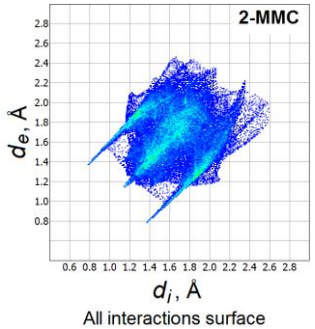

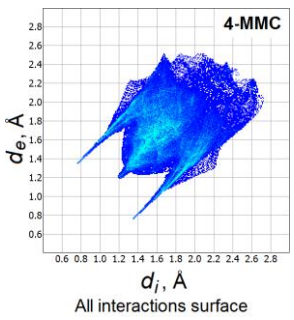

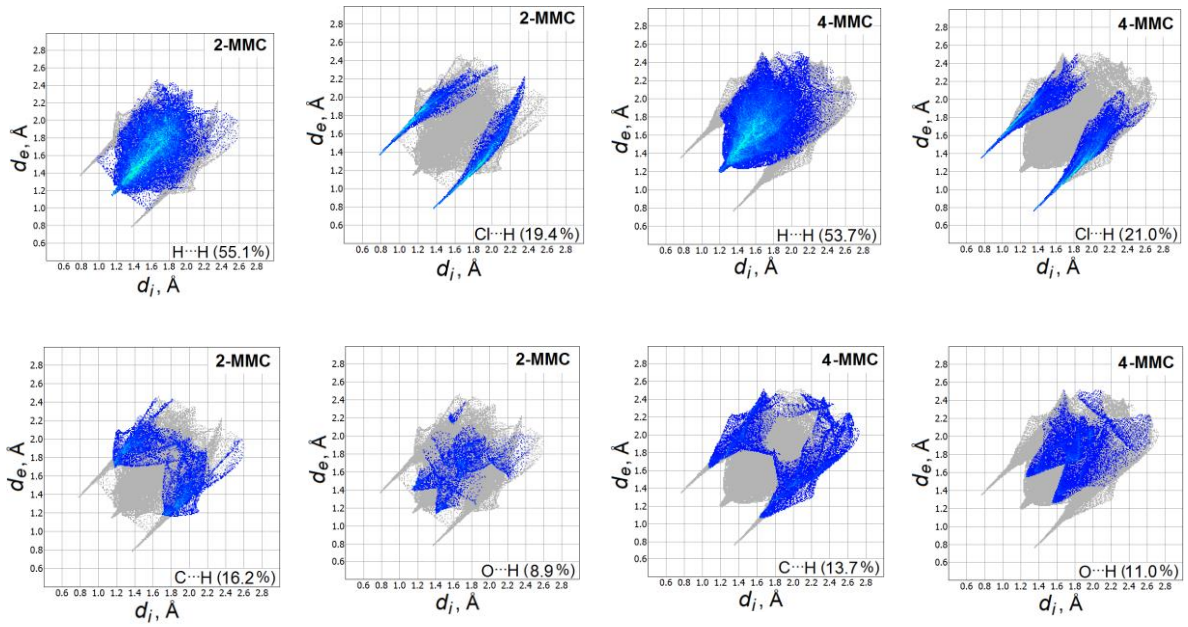

Figure 3. Fingerprint plots for 2-MMC and 4-MMC (The d_e and d_i denote the external and internal distances, respectively). The relative contributions of the particular intermolecular interactions on the HS (%) are presented in two low-lying rows.

3.2. Structural features in the 2- and 4-MMC·HCl dimers, DFT results.

The experimental 2- and 4-MMC dimer structures are shown in Figure 4. The optimized structures with the numbers of atoms specified by the program are shown in Figure S1 in Supplementary Information, SI. The calculated structural parameters were compared with the corresponding experimental data obtained by X-ray diffraction analysis of the compounds 2- and 4-MMC in Refs. [40,41]. Relevant structural data (bond lengths and angles) for the dimer 1 and 2 of the 2-methyl methcathinone hydrochloride and one dimer of the 4-methyl methcathinone hydrochloride are presented in Tables S1 and S2 in SI, selected intermolecular distances for the dimers 1 and 2 of 2-MMC·HCl are given in Table 1.

Both dimers of the 2-MMC compound, selected from the elementary cell, have close bond lengths, bond-, and torsion angles (Table S1 in SI), but different intermolecular distances between chlorine atoms and hydrogen and oxygen atoms of the neighboring molecule (Table 1). In the optimized dimers structures of the 2- and 4-MMC, the N–HCl and N–H bonds become longer; the C–H bonds of the methine groups are also stretched, and the H–Cl bonds become shorter (Table S1). This is because the dimer model does not take into account the equivalent intermolecular forces in all directions from the whole crystalline medium and leads to a different conformation of the molecule, which in this case, is the most energetically advantageous.

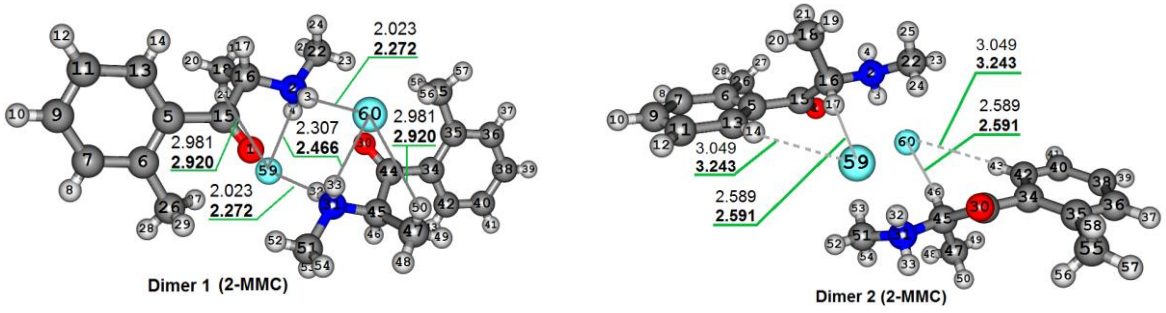

a

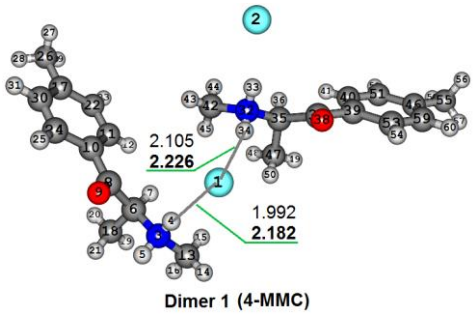

b

Figure 4. The structures of the corresponding dimers selected from crystals of 2-MMC (*a*) and 4-MMC (*b*). Selected bond lengths (Å) theoretically calculated (top number) and experimental (bottom number indicated in bold) values for the dimers. Oxygen atoms are in red color; Chlorine atoms are in turquoise; Nitrogen atoms are in blue.

The rest of the bond lengths, bond-, and torsion angles are well reproduced by quantum chemical calculations.

Table 1. Selected intermolecular distances (Å) for the dimer 1 and dimer 2 of 2-MMC·HCl calculated at the B3LYP/6-31G(d,p) theory level

Structural parameters	Dimer1		Dimer2	
	theor.	exp., [41]	theor.	exp., [41]
NH4 (**1**)···Cl 59 (**2**) NH33 (**2**)···Cl 60 (**1**)	2.307 2.307	2.466 2.466	4.736 4.777	5.044 5.044
NH3 (**1**)···Cl 59 (**2**) NH32 (**2**)···Cl 60 (**1**)	3.774 3.775	3.661 3.661	4.491 4.510	4.345 4.345
Cl 60 (**1**)···H50 (**2**) Cl 59 (**2**)···H21 (**1**)	2.981 2.981	2.920 2.920	5,176 5.177	5.066 5.066
H17 (**1**)···Cl 59 (**2**) H46 (**2**)···Cl 60 (**1**)	4.891 4.903	4.684 4.684	2.589 2.589	2.591 2.591
$H14_{Ar}$ (**1**)···Cl59 (**2**) $H43_{Ar}$ (**2**)···Cl60 (**1**)	6.162 6.201	5.930 5.930	3.049 3.049	3.243 3.243
O1 (**1**)···Cl 59 (**2**) O30 (**2**)···Cl 60 (**1**)	3.475 3.475	3.475 3.475	5.197 5.179	5.236 5.236

Number of molecules in the dimer are shown by bold digits in brackets.

Short intermolecular contacts NH···Cl and intramolecular contacts NH–Cl in dimers of the 2-MMC and 4-MMC (Table 1 and Tables S1 and S2 in SI), calculated with DFT/B3LYP/6-31G(d,p) approach, are in good agreement with the X-ray data. The Hirshfeld surfaces analysis of the intermolecular interactions for the crystalline 2-MMC compound. In the optimized structure of the 4-MMC dimer, as well as in the experiment [40], one short intermolecular contact NH34(2)···Cl 1(1) (calc.: 2.105 Å, exp.: 2.226 Å) and intramolecular contacts NH4–Cl 1 and NH33–Cl 2 (calc.: 1.992 and 1.993 Å, respectively, exp.: 2.182 Å) were found in notable disagreement. Thus, in the dimer 4-MMC structure, three N–H bonds are under the influence of chlorine atoms. Only one N3–H5 bond, which does not participate in the salt formation, can participate in the vibrational process as a free bond.

3.3. Bader's QTAIM analysis.

In order to characterize the non-covalent chemical interactions, the topological characteristics of the electron density were calculated for the 2- and 4-MMC dimers (Figure 4) at the (3, -1) critical points using the Bader's QTAIM approach. It was found that for both 2- and 4-MMC dimers, strong NH···Cl contacts take place (Figure 4). According to QTAIM analysis, these NH···Cl contacts have the positive values of the electron density Laplacian

$\nabla^2\rho(r) > 0$ and the negative values of the Cremer–Kraka electron energy density $h_e(r) < 0$; that allows us to classify these bonds as an intermediate type of interactions (Table 2). Another two parameters, namely bond ellipticity (ε) and delocalization index (DI) can shed light on the bonding characteristics in 2- and 4-MMC dimers. Large ellipticity values indicate structural instability and *vice versa*. All NH···Cl contacts have reasonably small ellipticity values (Table 2), indicating cylindrically symmetrical bonds and dynamically stable binding character of the $NH2^+$–Cl^- salt fragments. The delocalization index values elaborate on this bonding nature and determine the measure of the electron density concentration in the interatomic region. In the case of the 2-MMC dimer, the total energy values of the NH···Cl contacts estimated by the EML formula (Eq. 6) are –8.53 kcal mol^{-1} for NH32–Cl 59/NH3–Cl 60 and –4.20 kcal mol^{-1} for NH4···Cl 59/NH33···Cl 60 contacts (Table 2). For the 4-MMC dimer, the energy of the NH···Cl contacts is –11.23 kcal mol^{-1} for the NH4–Cl 1 link and –7.15 kcal mol^{-1} for the NH34···Cl 1 contact (Table 2).

Table 2. Topological characteristics of the non-covalent bonds calculated by the QTAIM method for the 2- and 4-MMC dimers.

Bond	*d*, Å	$\rho(\mathbf{r})$, $e \cdot a_o^{-3}$ [1]	$v(\mathbf{r})$, a.u.	$g(\mathbf{r})$, a.u.	$h_e(\mathbf{r})$, [2] a.u.	$\nabla^2\rho(\mathbf{r})$, $e \cdot a_o^{-5}$	*E*, kcal/mol	ε	DI
2-MMC (Dimer 1)									
NH32–Cl59 NH3–Cl60	2.023 **2.272**	0.0405	–0.0272	0.0221	–0.0051	0.0676	–8.53	0.0118	0.174
NH4 (**1**)···Cl59 (**2**) NH33 (**2**)···Cl 60 (**1**)	2.307 **2.466**	0.0223	–0.0134	0.0127	–0.0007	0.0483	–4.20	0.0322	0.115
Cl59 (**2**)···H21C18 (**1**) Cl60 (**1**)···H50C47 (**2**)	2.981 **2.920**	0.0067	–0.0030	0.0040	0.0010	0.0201	–0.94	0.0268	0.043
2-MMC (Dimer 2)									
Cl59 (**2**)···H17C16 (**1**) Cl60 (**1**)···H46C45 (**2**)	2.589 **2.591**	0.0134	–0.0074	0.0083	0.0009	0.0363	–2.32	0.0250	0.085
4-MMC (Dimer 1)									
NH4–Cl1	1.992 **2.182**	0.0495	–0.0358	0.0273	–0.0085	0.0753	–11.23	0.0079	0.196
NH34(**2**)···Cl1 (**1**)	2.105 **2.226**	0.0329	–0.0228	0.0202	–0.0026	0.0705	–7.15	0.0303	0.133

[1] a_0 is the Bohr radius; [2] $h_e(\mathbf{r}) = v(\mathbf{r}) + g(\mathbf{r})$, where $g(\mathbf{r})$ is the kinetic energy density at the (3, –1) critical point;$1/4\nabla^2\rho(\mathbf{r}) = 2g(\mathbf{r}) + v(\mathbf{r})$. Experimental X-ray data [40, 41] are highlighted in bold. Bold symbol denotes the number of molecule in the dimer.

Both 2- and 4-MMC crystals are also stabilized by weak closed-shell non-covalent CH···Cl contacts, which were predicted in dimers with $\nabla^2\rho(r) > 0$ and $h_e(r) > 0$ (Table 2). In the 2-MMC crystal, each chlorine atom is held by the two CH···Cl bonds (dimers 1 and 2), characterized by relatively small ellipticity values and a low concentration of electron density in the inter-atomic space (Table 2). The bond energy of CH···Cl contacts in 2-MMC is in the range of (–2.32 till –0.94) kcal mol^{-1} (Table 2). The 4-MMC crystal also contains weak CH···Cl contacts (2.643 Å and 2.867 Å, Figure 2) with an energy of about 2 kcal mol^{-1}.

Thus, the topological consideration of the 2- and 4-MMC dimers allows the prediction of electronic peculiarities for the non-covalent bonds occurring in crystals. The presence of NH···Cl and CH···Cl contacts mainly contributes to a specific arrangement of molecules in the 2- and 4-MMC crystal packing.

3.4. IR spectra of the 2- and 4-MMC dimers.

Numerical values of some vibrational frequencies and IR absorption intensities, together with their assignment in the calculated IR spectrum of 2-MMC (dimer 1 and dimer 2) and 4-MMC dimer, are shown in Tables 3 and 4. The complete Tables for all calculated modes are presented in Tables S3–S5 in SI.

Table 3. Calculated frequencies, IR intensities, experimental data, and assignment of selected vibrational modes for the dimer 1 and dimer 2 of 2-MMC·HCl determined at the B3LYP/6-31G(d,p) theory level.

Dimer 1		**Dimer 2**		**Exp. [37]**	**Assignment**
DFT freg. calc.	I_{IR}	**DFT freq. calc.**	I_{IR}		
–	–	3387	59	3372 [41]	N–H4 str., **1**
–	–	3379	65	3372 [41]	N–H33 str., **2**
3037	23	3034	34	3024	C–H_{Ar} str., **2**
3024	25	3018	14	3024	C–H_{Ar} str., **1**
2996	10	2997	4	2984	CH_3 str., as., **2**
–	–	2985	132	2984	$C42_{Ar}$–H43 str. (**2**)···Cl 60 (**1**)
–	–	2984	92	2984	$C13_{Ar}$–H14 str. (**1**)···Cl 59 (**2**)
2961	22	2962	15	2959	$CH_{3\ Ar}$ str., as., **2**
2960	19	2962	17	2959	$CH_{3\ Ar}$ str., as., **1**
2933	110	–	–	2920	$C22H_3$str., s.,**1**,N–H4 (**1**)···Cl 59 (**2**) str., $C51H_3$str., s., **2**, N–H33 (**2**)···Cl 60 (**1**) str., ooph.
–	–	2933	6	2920	$C22H_3$ str., s., **1**
–	–	2932	6	2920	$C51H_3$ str., s., **2**
2899	51	2895	8	2895	$C18H_3$ str., s., **1**, $C47H_3$ str., s., **2**
2882	35	2887	21	2895	$CH_{3\ Ar}$ str., s., **1**
2882	12	2887	21	2895	$CH_{3\ Ar}$ str., s., **2**
–	–	2878	158	2895	C45–H46 str. (**2**)···Cl 60 (**1**)
–	–	2876	83	2895	C16–H17 str. (**1**)···Cl 59 (**2**)
2774	280	–	–	2742	N–H4 (**1**)···Cl 59 (**2**) str., C16–H17 str., **1**, N–H33 (**2**)···Cl 60 (**1**) str., C45–H46 str., **2**
2753	256	–	–	2742	N–H4 (**1**)···Cl 59 (**2**) str., C16–H17 str., **1**, N–H33 (**2**)··· Cl 60 (**1**) str., C45–H46 str., **2**
–	–	2451	749	2451	N–H3–Cl 60 str., **1**, N–H32–Cl 59 str., **2**, ooph.
–	–	2364	109	2361	N–H3–Cl 60 str., **1**, N–H32–Cl 59 str., **2**, iph.
2458	805	–	–	2451	N–H3–Cl 60 str., **1**, N–H32–Cl 59 str., **2**, ooph., N–H4 (**1**)···Cl 59 (**2**) str., **1**, N–H33 (**2**)···Cl 60 (**1**) str., **2**
2419	4	–	–	2361	N–H3–Cl 60 str., **1**, N–H32–Cl 59 str., **2**, iph., N–H4 (**1**)···Cl 59 (**2**) str., **1**, N–H33 (**2**)···Cl 60 (**1**) str., **2**
1714	272	1691	224	1696	C=O str., NH_2 scis., **1**, **2**, ooph.
1712	113	1691	92	1696	C=O str., NH_2 scis., **1**, **2**, iph.
1621	0.004	–	–	–	NH_2 scis., **1**, **2**, iph.
1591	17	1606	18	1600	C=C str., s., **2**
1591	12	1606	19	1600	C=C str., s., **1**
1571	35	1574	42	1572	NH_2 scis., **1**, **2**, ooph.
1558	9	1536	85	1550	C=C str., s., **1**
1558	52	1536	38	1550	C=C str., s., **2**
1470	0.2	1488	31	1489	C=C str., as., **2**
1467	9	1487	30	1489	C=C str., as., **1**
1459	122	1463	43	1459	CH_3 def., as., NH_2 wag., **1**,**2**, ooph.
1450	93	1452	88	1459	CH_3 def., as., NH_2 wag., **1**,**2**, ooph.
1427	95	1430	47	1430	CH_3 def., as., NH_2 wag., **1**, **2**
1418	23	1419	1	1417	C=C str., as., $CH_{3\ Ar}$def., as., **1**, **2**

Dimer 1		Dimer 2		Exp. [37]	Assignment
DFT freg. calc.	I_{IR}	DFT freq. calc.	I_{IR}		
1376	42	1388	55	1380	CH_3 def., s., NH_2twist., **1**, **2**
–	–	1336	15	1336	NH_2 twist., CH bend.,**1**, **2**
1308	30	1294	8	1300	NH_2 twist., CH bend.,**1**, **2**
1293	12	1294	17	1300	C=C str., as. Kekule, **1**, **2**
1292	12	1293	13	1300	C=C str., as. Kekule, **1**, **2**
1268	34	–	–	1246	C_{Ar}–C str., **1**,**2**, ooph., CCH_{Ar} bend, CH bend.
1221	54	1220	70	1200	C_{Ar}–C str., CH bend., **1**, **2**, iph.
1191	155	1220	123	1200	C_{Ar}–C str., CH bend., **1**, **2**, ooph.
1094	68	1101	124	1095	C–N str., CH bend., CH_3 twist., **1**, **2**, ooph.
1048	15	1042	7	1049	$CH_{3\ Ar}$ rock., **1**, **2**
1034	14	1031	26	1030	C–CH_3 str., N–CH_3str., C–N str., **1**
–	–	1005	7	1007	N–CH_3 str., C–N str., ooph., CCH_{Ar} oop. bend., **2**
1013	43	–	–	1007	C–CH_3 str., N–CH_3str., ooph., **1**, **2**
970	143	971	30	973	C–C str., CH_{Ar} oop. bend., CH_3 rock., **2**
–	–	942	137	947	C–C str., ring def., CH_3 rock., CCH_{Ar} oop. bend., **1**
944	13	–	–	947	CCH_{Ar} oop. bend., **2**
852	11	850	30	845	C–N str., **1**, **2**, ooph.
788	11	786	28	781	CCH_{Ar} oop. bend., **1**.
755	40	755	47	752	CCH_{Ar} oop. bend., **1**, **2**, ooph.
732	16	726	12	728	CCH_{Ar} oop. bend., iph., **2**
675	13	671	11	671	CCH_{Ar} oop. bend., **1**
641	7	634	1	636	Ring def., ip., as., CNC bend., **2**
568	3	560	6	564	Ring def., ip., as., CNC bend., **2**
526	12	527	25	524	CCH_{Ar} oop. bend., **2**

Abbreviations: DFT freq. calc.. – calculated frequency with scale factor, cm^{-1}; exp. – experimental; I_{IR} – calculated IR intensity, km/mol; Ar – aryle; def. – deformation; str. – bond stretching; rock. – rocking, twist. – twisting, wag. – wagging, bend. – bending, scis. – scissoring deformation vibrations; s. – symmetric and as. − asymmetric vibrations; ooph. – out-of-phase; iph. – in-phase; ip. – in-plane; oop. – out-of-plane.
The bold symbol denotes the number of molecules in dimer 1.

Table 4. Calculated frequencies, IR intensities, experimental date, and assignment of selected vibrational modes for the dimer of 4-MMC·HCl determined at the B3LYP/6-31G(d,p) theory level

Mode	DFT freq. calc.	Exp. [37]	I_{IR}	Assignment
ν_{174}	3358	3356 [40]	40	N3–H5 str., **1**
ν_{173}	3092		2	C–H_{Ar} str., iph., **2**
ν_{172}	3088		4	C–H_{Ar} str., iph., **1**
ν_{171}	3078	3065	13	C–H_{Ar} str., iph., **2**
ν_{169}	3065	3065	11	C–H_{Ar} str., iph., **1**
ν_{168}	2999	3000	13	C–H_{Ar} str., ooph., **2**
ν_{167}	2997	3000	18	C–H_{Ar} str., ooph., C13H_3str., as., **1**
ν_{166}	2996	3000	18	C–H_{Ar} str., ooph., C13H_3str., as., **1**
ν_{165}	2995	3000	12	C–H_{Ar} str., ooph., **2**
ν_{164}	2995	3000	8	C42H_3 str., as., **2**
ν_{163}	2994	3000	14	C–H_{Ar} str., ooph., **1**
ν_{161}	2970	2967	11	C18H_3 str., as., **1**
ν_{160}	2966	2967	15	C47H_3 str., as., **2**
ν_{159}	2961	2967	9	C47H_3 str., as., **2**
ν_{158}	2951	2942	5	C18H_3 str., as., **1**
ν_{157}	2950	2942	14	C55$H_{3\ Ar}$ str., as., **2**
ν_{156}	2946	2942	16	C26$H_{3\ Ar}$ str., as., **1**
ν_{155}	2920	2917	14	C55$H_{3\ Ar}$ str., as., **2**
ν_{154}	2917	2917	19	C26$H_{3\ Ar}$ str., as., **1**
ν_{153}	2914	2904	25	C42H_3 str., s., C35–H36 str., **2**
ν_{152}	2909	2904	12	C42H_3 str., s., C35–H36 str., **2**

Mode	DFT freq. calc.	Exp. [37]	I_{IR}	Assignment
ν_{151}	2878	2871	41	$C13H_3$ str., s., C6–H7 str., **1**
ν_{150}	2866	2871	10	$C47H_3$ str., s., **2**, C6–H7 str., **1**
ν_{149}	2756	2740	121	N32–H34 (**2**)···Cl 1(**1**) str.
ν_{148}	2743	2740	184	N32–H34 (**2**)···Cl 1(**1**) str.
ν_{147}	2738		18	$C55H_{3\,Ar}$ str., s., **2**
ν_{146}	2734	2740	165	N32–H34 (**2**)···Cl 1(**1**) str.
ν_{145}	2734	2740	389	N32–H34 (**2**)···Cl 1(**1**) str.
ν_{144}	2458	2451	805	N3–H4–Cl 1 str., **1**, N32–H33–Cl 2 str., **2**, ooph.
ν_{143}	2410	2418	131	N3–H4–Cl 1str., **1**, N32–H33–Cl 2 str., **2**, iph.
ν_{142}	1716	1684	161	C=O str., $N32H_2$scis., **2**
ν_{141}	1689	1684	190	C=O str., $N3H_2$scis., **1**
ν_{140}	1606	1605	72	C53=C59 and C40=C51 str., s., **2**
ν_{139}	1606	1605	107	C24=C30 and C11=C22 str., s., **1**
ν_{138}	1578	1569	34	$N32H_2$ scis., **2**
ν_{137}	1562	1569	10	C39=C40 and C59=C46 str., s., **2**
ν_{136}	1562	1569	11	C10=C11 and C30=C17 str., s., **1**
ν_{135}	1542	1569	95	$N3H_2$ scis., **1**
ν_{134}	1502	1492	2	C=C str., as., **1**
ν_{133}	1497	1492	1	C=C str., as., **2**
ν_{132}	1485	1467	85	$C42H_3$ def., as., $N32H_2$ wag., **2**
ν_{131}	1474	1467	25	$C13H_3$ def., as., $N3H_2$ wag., **1**
ν_{130}	1472	1467	28	$C42H_3$ def., as., $C47H_3$ def., as., **2**
ν_{129}	1472	1467	5	$C13H_3$ def., as., $C18H_3$ def., as., **1**
ν_{128}	1461	1457	12	$C47H_3$ def., as., **2**
ν_{127}	1458	1457	3	$C13H_3$ def., as., $C18H_3$ def., as., **1**, $C42H_3$ def., as., $C47H_3$ def., as., $N32H_2$ twist., **2**
ν_{126}	1457	1457	31	$C42H_3$ def., as., $C47H_3$ def., as., $N32H_2$ twist., **2**, $C13H_3$ def., as., $C18H_3$ def., as., $N3H_2$ twist., **1**
ν_{124}	1453	1457	9	$C55H_{3Ar}$ def., as., **2**
ν_{123}	1452	1457	10	$C26H_3$ def., as., **1**
ν_{122}	1449	1457	14	$C13H_3$ def., as., $C18H_3$ def., as., $N3H_2$ twist., C6H7 bend, **1**
ν_{119}	1437	1457	8	$C42H_3$ def., as., $N3H_2$ wag., **2**
ν_{118}	1423	1412	18	$C13H_3$ def., s., $C18H_3$ def., s., $N3H_2$ wag., C6H7 bend., **1**
ν_{117}	1412	1412	6	$C13H_3$ def., s., $C18H_3$ def., s., $N3H_2$twist., C6H7 bend., **1**
ν_{115}	1400	1412	13	C53=C59 and C40=C51 str., as., $N32H_2$ twist., C35H36 bend., **2**
ν_{114}	1398	1412	21	C24=C30 and C11=C22 str., as., $N3H_2$ twist., C6H7 bend., **1**
ν_{113}	1382	1384	83	$C47H_3$ def., s., $N32H_2$ twist., C35H36 bend., **2**
ν_{111}	1376	1384	22	$C47H_3$ def., s., $N32H_2$ twist., **2**
ν_{108}	1330	1347	42	$N32H_2$ twist., C35H bend, **2**
ν_{107}	1310	1295	9	C=C str., as. Kekule, **1**
ν_{105}	1308	1295	94	Ring str., C6–C8 str., C6H7 bend., $N3H_2$ twist., **1**
ν_{104}	1299	1295	25	Ring str., C6–C8 str., C6H7 bend., $N3H_2$ twist., **1**
ν_{103}	1294	1295	7	Ring str., C35H bend., **1**
ν_{102}	1288	1295	15	C6H7 bend., C6–C8 str., C8–$C10_{Ar}$ str., ooph., $N3H_2$ twist., **1**
ν_{101}	1280	1295	43	C35H36 bend., C35–C37 str., C37–$C39_{Ar}$str., ooph., **2**
ν_{100}	1256	1248	107	C8–$C10_{Ar}$ str., C6–N3 str., C6H bend., **1**
ν_{99}	1236	1248	121	C37–$C39_{Ar}$ str., C35–N32 str., C35H bend., **2**
ν_{97}	1213	1215	17	$C55H_3$–$C46_{Ar}$ str., CCH_{Ar} bend., **2**
ν_{95}	1196	1201	20	CCH_{Ar} bend., $N32H_2$ rock., 2, CCH_{Ar} bend., **1**
ν_{94}	1194	1201	13	CCH_{Ar} bend., NH_2 rock., **1**, **2**
ν_{93}	1186	1189	34	CCH_{Ar} bend., $N32H_2$ rock., **2**
ν_{92}	1164	1166	5	C6–N3 str., C6H7 bend., $C13H_3$ rock., **1**
ν_{91}	1160	1166	7	C35–N32 str., C35H36 bend., $C42H_3$ rock., **2**
ν_{90}	1128	1126	13	CCH_{Ar} bend., **1**
ν_{89}	1126	1126	12	CCH_{Ar} bend., **2**
ν_{88}	1098	1096	50	C35–N32 str., N32–$C42H_3$ str., ooph., $C47H_3$ rock., $C42H_3$ rock., **2**
ν_{87}	1097	1096	25	C6–N3 str., N3–$C13H_3$ str., ooph., $C13H_3$, $C18H_3$ rock., **1**
ν_{86}	1058	1050	8	N32–$C42H_3$str., C35–$C47H_3$str., $N32H_2$ twist., **2**
ν_{83}	1052	1050	13	$C26H_3$ rock., **1**
ν_{82}	1048	1050	13	C35–N3 str., N32–$C42H_3$ str., ooph., C35–$C47H_3$str., **2**
ν_{81}	1035	1030	15	C6–N3 str., N3–$C13H_3$ str., ooph., C6– $C18H_3$ str., **1**
ν_{78}	1013	1008	21	N32–$C42H_3$ str., $C47H_3$ rock., $C55H_3$ rock., **2**
ν_{77}	1008	1008	14	N3–$C13H_3$ str., $C18H_3$ rock., $C26H_3$ rock., **1**
ν_{76}	1006	1008	40	$C55H_3$ rock., N32–$C42H_3$ str., **2**

Mode	DFT freq. calc.	Exp. [37]	I_{IR}	Assignment
ν_{75}	1005		8	$C26H_3$ rock., N3–$C13H_3$ str., **1**
ν_{74}	990 sh.	976	6	CH_{Ar} oop. bend., ooph., **1**, **2**
ν_{73}	988 sh.	976	17	CH_{Ar} oop. bend., ooph., **1**, **2**
ν_{71}	978	976	42	CH_{Ar} oop. bend., ooph., C6–C8 str., N3–$C13H_3$str., iph., $C18H_3$ rock., **1**
ν_{70}	973	976	48	CH_{Ar} oop. bend., ooph., C35–C37 str., N32–$C42H_3$str., iph., $C47H_3$ rock., **2**
ν_{68}	912	889	35	$N32H_2$ rock., **2**
ν_{67}	863	889	41	$N3H_2$, rock., **1**
ν_{66}	851	854	4	CH_{Ar} oop. bend., ooph., **1**, **2**
ν_{65}	848	854	6	CH_{Ar} oop. bend., ooph., **1**, **2**
ν_{64}	841	854	4	N32–C35 str., ring breathing, **2**
ν_{63}	836	844	20	CH_{Ar} oop. bend., iph., **1**
ν_{62}	824	828	12	CH_{Ar} oop. bend., iph., **2**
ν_{61}	822	828	16	N3–C6 str., ring breathing, **1**
ν_{60}	802	802	5	$C46_{Ar}$–$C55H_3$ str., ring str., s., **2**
ν_{59}	801	802	8	$C17_{Ar}$–$C26H_3$ str., ring str., s., **1**
ν_{58}	753	757	18	CCH_{Ar} oop. bend., iph., **1**
ν_{57}	746	757	9	CCH_{Ar} oop. bend., iph., **2**
ν_{56}	735	733	10	CCH_{Ar} oop. bend., iph., **1**
ν_{55}	731	733	8	CCH_{Ar} oop. bend., iph., **2**
ν_{54}	688	687	6	Ring def., oop, **1**
ν_{53}	682	687	4	Ring def., oop, **2**
ν_{50}	599	600	7	Ring def., ip., s., **1**
ν_{49}	598	600	3	Ring def., ip., s., **2**
ν_{48}	512	510	5	$N3H_2^+$ libration movement relative Cl 1 atom, **1**
ν_{47}	507	510	18	$N32H_2^+$ libration movement relative Cl 2 atom, **2**
ν_{46}	480	478	8	CCH_{Ar} oop. bend., iph., **1**
ν_{45}	480	478	18	CCH_{Ar} oop. bend., iph., **2**

Abbreviations: DFT freq. calc. – calculated frequency with scale factor, cm^{-1}; exp. – experimental; I_{IR} – calculated IR intensity, km/mol; Ar – aryle; def. – deformation; str. – bond stretching; rock. – rocking, twist. – twisting, wag. – wagging, bend. – bending, scis. – scissoring deformation vibrations; s. – symmetric and as. − asymmetric vibrations; ooph. – out-of-phase; iph. – in-phase; ip. – in-plane; oop. – out-of-plane.
The bold symbol denotes the number of molecules in the dimer.

The calculated and experimental IR spectra for the dimers 1 and 2 of 2-MMC·HCl in the high-frequency region are presented in Figure 5, and for the dimer 4-MMC·HCl – in Figure 6.

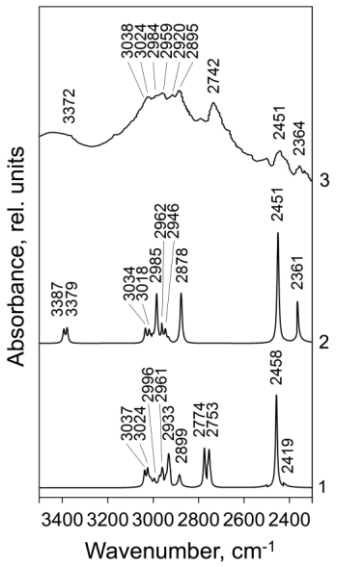

Figure 5. Calculated (curves 1 and 2) and experimental (curve 3, [37]) IR spectra of 2-methyl methcathinone hydrochloride in the 3500–2300 cm^{-1} range: curve 1 – IR spectrum for dimer 1, curve 2 – IR spectrum for dimer 2. Line half-width is 5 cm^{-1}.

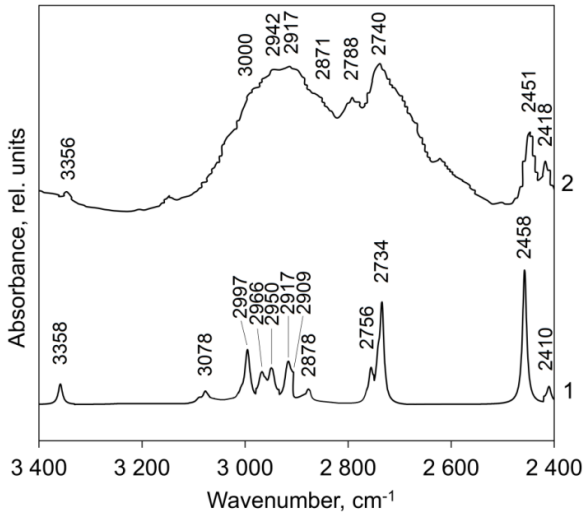

Figure 6. Calculated (curve 1) and experimental (curve 2, [37]) IR spectra of 4-methyl methcathinone hydrochloride in the 3500–2300 cm^{-1} range. Line half-width is 5 cm^{-1}.

The highest frequencies in the calculated IR spectra of 2-MMC·HCl (Figure 5, curve 2) show weak bands ν(N2–H4) and ν(N31–H33) stretching vibrations (calc.: 3387 and 3379 cm^{-1}). These normal vibrations happen only in dimer 2, where the hydrogen atoms H4 and H33 connected with nitrogen are located far from hydrogen chloride (Figure 4); thus, they do not interact with HCl. The corresponding absorption band in the experimental IR spectrum does not have a clearly defined maximum (Figure 5), and therefore, different values are given in different Refs for ν(N–H) in 2-MMC·HCl compound: 3372 cm^{-1} [41], 3443.5 cm^{-1} [37]. In the IR spectrum of 4-MMC, the absorption of the free N–H group was calculated at 3358 cm^{-1} (exp.: 3356 cm^{-1} [40], Figure 6).

In the experimental IR spectrum of the 2-MMC·HCl compound, absorption in the range 3000–2800 cm^{-1} appears as a complex band with weakly pronounced peaks (Figure 5, curve 3). The weak peak at 3024 cm^{-1} and left shoulder are related to valence vibrations of C–H bonds in the aromatic ring (calc.: 3037, 3024 cm^{-1} in dimer 1 and 3034, 3018 cm^{-1} in dimer 2, Figure 5, curves 1 and 2, respectively, Table 3). The peak at 2959 cm^{-1} and left shoulder (2984 cm^{-1}) belong to asymmetric vibrations of methyl groups (calc.: 2996, 2961 in dimer 1 and 2997, 2962 cm^{-1} in dimer 2); in this case, the absorption by the methyl group of the aromatic ring occurs at lower frequencies (Tables S3 and S4 in SI). A very weak absorption band of asymmetric vibrations of CH_3 groups at 2997 cm^{-1} in dimer 2 is overlapped by an intense absorption band at 2985 cm^{-1} of C–H valence vibrations ($C42_{Ar}$–H43 and $C13_{Ar}$–H14 in the aromatic ring, which is under the influence of the chlorine atom from the HCl counterpart from the other molecule); the calculated intermolecular distances $H14_{Ar}$ (1)···Cl 59 (2) and $H43_{Ar}$ (2)···Cl 60 (1) are equal 3.049 Å (exp.: 3.243 Å, Table 1). Such weak contact is also predicted by Hirshfeld surfaces analysis of the intermolecular interactions for crystalline 2-MMC compound (Figure 2).

Symmetric vibrations of methyl groups were calculated in the range 2933–2882 cm^{-1} (Tables S3 and S4 in SI). Therefore, the experimental peaks at 2920 and 2895 cm^{-1} were assigned to these symmetrical CH_3 vibrations.

In the IR spectrum of isolated dimer 2 the strong absorption band of methine groups C16–H7 and C45–H46 (Figure 5, Table 3) was calculated at 2878 cm^{-1}. Although the methine group has a relatively weak absorption [66], such strong IR absorption is determined by the presence of chlorine atom from the neighboring molecule in the vicinity of H7 and H46 atoms

of methine groups in the 2-MMC dimer (Figure 4). As stated above, the C–H···Cl interactions between methine groups and the chlorine atoms of the neighboring molecule provide short contacts with distances of 2.591 Å in 2-MMC crystals (calc.: 2.589 Å in the isolated dimer 2). Dimer 1 has no short contact between methine groups and the chlorine atoms of the neighboring molecule (Table 1). We paid attention to weak contacts between H21, and H50 atoms of the $C18H_3$ and $C47H_3$ methyl groups with the chlorine atom of the neighboring molecules identified in the Hirshfeld surfaces analysis of the intermolecular interactions for crystalline 2-MMC compound and determined by the Bader's QTAIM analysis for the optimized structure of dimer 1 (calculated intermolecular distances H21 (1)···Cl 59 (2) and H50 (2)···Cl 60 (1) are equal 2.98 Å, exp.: 2.92 Å [41], Table 1). They are manifested differently in the IR spectrum for two dimer models (they are seen only in symmetric C–H vibrations of methyl groups $C18H_3$ and $C47H_3$). The absorption intensity in dimer 1 is approximately 6 times stronger (51 km/mol) compared to dimer 2 (8 km/mol, Table 3, $\nu_{calc.}$= 2899 cm^{-1}, $\nu_{exp.}$= 2895 cm^{-1}).

Interaction of a free NH group (not bound to HCl) with a chlorine ion of a neighboring molecule produces strong bands of valence vibrations N–H (1)···Cl (2) and N–H (2)···Cl (1) in the IR spectrum of the dimer 1 of 2-MMC at 2774 and 2753 cm^{-1} (Table 3, Figure 5). This interaction is determined by the shortest intermolecular contacts NH4 (1)···Cl 59 (2) and NH33 (2)···Cl 60 (1) (calc.: 2.31 Å, exp.: 2.46 Å, Table 3). In our opinion, a strong band at 2742 cm^{-1} in the experimental IR spectrum of 2-MMC is due to this interaction. The intermolecular distances NH4 (1)···Cl 59 (2) and NH33 (2)···Cl 60 (1) for the dimer 2 of 2-MMC·HCl are too large (exp.: 5.044 Å, Table 3), and therefore these types of vibrations are absent in the IR spectrum of the dimer 2. At the same time, a short intermolecular contact NH34 (2)···Cl·1 (1) (calc.: 2.105 Å, exp.: 2.226 Å) in 4-MMC dimer gives a strong IR absorption band 2734 cm^{-1} and a weak band at 2756 cm^{-1} (exp.: 2740 and 2788 cm^{-1}, respectively).

The band at 2933 cm^{-1}, theoretically calculated in the IR spectrum of the dimer 1, which we attributed to symmetric vibrations of C–H bonds of methyl groups, also has a contribution from valence vibrations N–H (1)···Cl (2) and N–H (2)···Cl (1) and increased absorption intensity (110 km/mol, Table 3).

The calculated spectrum of 4-MMC compound in the high-frequency region shows characteristic ν(C–H) stretching bands of the aromatic rings at 3078 cm^{-1} (exp.: 3065 and 3000 cm^{-1}), ν_{as} CH_3 at 2997, 2966, 2950, and 2917 cm^{-1} (exp.: 3000, 2942, and 2917 cm^{-1}), ν_s CH_3 and ν(C–H) stretching of the methine groups at 2909 and 2878 cm^{-1} (exp.: 2871 cm^{-1}, Figure 6, Table S5 in SI). All the spectrum is well reproduced by one dimer model for the 4-MMC compound.

For the 2-MMC crystal model, the most strong bands, 2458 and 2451 cm^{-1} in the calculated spectra of dimers 1 and 2, respectively (Figure 5, curves 1 and 2), are produced by valence vibration of the intramolecular N–H–Cl fragments in both molecules of the dimers being in the out-of-phase relationships (mode of one molecule is out-of-phase to displacement in the other molecule). The corresponding absorption band in the IR spectrum of the 4-MMC dimer was also calculated at 2458 cm^{-1}. In the experimental spectra of 2- and 4-MMC, this vibration is observed at 2451 cm^{-1} and has significantly lower IR absorption (Figures 5, 6). The absorption associated with the salt type N–H–Cl vibrations in both molecules "in-phase" (calc.: 2419 and 2361 cm^{-1}, exp.: 2364 cm^{-1} for 2-MMC, Figure 5; calc.: 2410 cm^{-1}, exp.: 2418 cm^{-1} for 4-MMC, Figure 6) is much weaker in the calculated and experimental spectra of the studied compounds. Normal vibrations of the N–H–Cl fragment calculated at 2458 and 2419 cm^{-1} in the IR spectrum of the dimer 1 for 2-MMC have a contribution of valence vibrations N–H

(1)···Cl (2) and N–H (2)···Cl (1). The correct assignment of the IR bands in the range of 2800–2350 cm^{-1} for the 2- and 4-MMC compounds is confirmed by the fact that in the experimental IR spectrum of the vaporous sample of 4-MMC (base) [36] and our previous calculated spectra for the non-salt 4-MMC molecule (without hydrochloride) [42], these bands are absent at all.

The calculated and experimental IR spectra in the middle "fingerprint" frequency region (1800–500 cm^{-1}) are shown in Figure 7 for 2-MMC·HCl and Figure 8 for 4-MMC·HCl compounds.

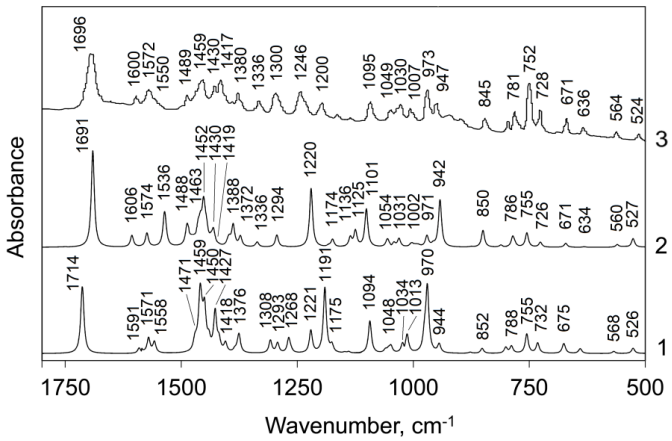

Figure 7. Calculated (curves 1, 2) and experimental (curve 3 [37]) IR spectra of 2-methyl methcathinone hydrochloride in the 1800–500 cm^{-1} range: curve 1 – IR spectrum for dimer 1, curve 2 – IR spectrum for dimer 2. Line half-width is 4 cm^{-1}.

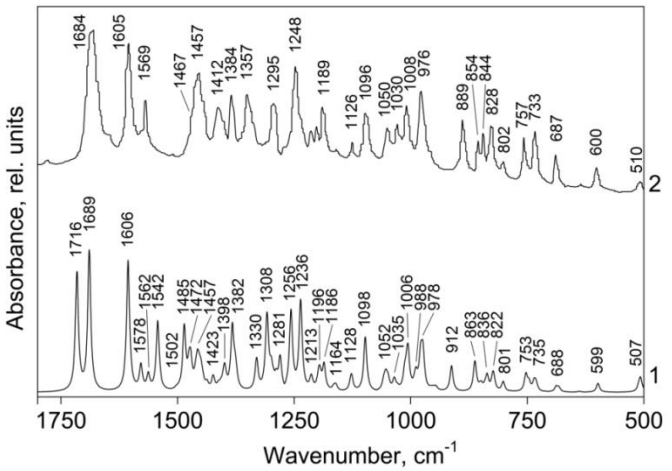

Figure 8 Calculated (curve 1) and experimental (curve 2 [37]) IR spectra of 4-methyl methcathinone hydrochloride in the 1800–500 cm^{-1} range. Line half-width is 4 cm^{-1}.

The calculated IR spectra of 2-MMC in the middle frequency region showed strong C=O absorption bands at 1714 and 1691 cm^{-1} for dimers 1 and 2, respectively (Figure 7, curves 1 and 2, exp.: 1696 cm^{-1}, curve 3). Here again, as in the case of the high-frequency region, the observed 2-MMC spectrum can be represented as a superposition of IR bands produced by both dimer models. The C=O absorption band for the 4-MMC dimer compound splits to form two bands at 1716 and 1689 cm^{-1} (exp.: 1684 cm^{-1}, Figure 8). The carbonyl groups ν(C=O) valence vibrations are mixed with scissoring deformation vibrations of amino groups (Tables 3 and 4). The NH_2 scissoring vibrations in the 4-MMC spectrum are rather weak (1569 cm^{-1}); for dimer 1 of the 2-MMC compound, it is also calculated at 1621 cm^{-1}, but has no intensity (*I* = 0.004 km/mol, Table 3). We also assigned the weak band at 1572 cm–1 in the experimental spectrum of 2-MMC (Figure 7, curve 3) to NH_2 scissoring vibrations (calc.: 1571 and 1574

cm^{-1} for dimers 1 and 2, respectively). These scissoring vibrations of the NH_2 group in the IR spectrum of 4-MMC are calculated at 1578 cm^{-1} (in molecule 2) and at 1542 cm^{-1}(in molecule 1) (exp.: 1569 cm^{-1}, Figure 8). The significant discrepancy in frequencies and intensities of scissoring vibrations of the NH_2 group in the IR spectrum of the 4-MMC dimer is because, in molecule 2 of the dimer, the NH_2 group is under the influence of two chlorine atoms, while in molecule 1 there is only one influencing Cl atom (Figure 4b).

The weak intensity band 1600 cm^{-1} and the right shoulder 1550 cm^{-1} at the band 1572 cm^{-1} in the experimental spectrum of 2-MMC (Figure 7, curve 3) are assigned to symmetric valence vibrations of the aromatic C=C bonds (calc.: 1591 and 1558 cm^{-1} in the IR spectrum of the dimer 1, Figure 7, curve 1; 1606 and 1536 cm^{-1} in the dimer 2, curve 2). Asymmetric C=C vibrations in the phenyl ring produce the weak intensity experimental band 1489 cm^{-1} (calc.: 1488 cm^{-1}) and give contributions to the medium intensity band 1417 cm^{-1} (1418 cm^{-1} in the IR spectrum of the dimer 1 and 1419 cm^{-1} in dimer 2). The reduction of experimental frequency of the band 1417 cm^{-1} (and the calculated as well) in comparison with standard characteristic group frequency of aromatic C=C bonds [66] we explained by the substituent influence (methyl group) in the aromatic ring. The aromatic C=C bonds vibrations in the spectrum of 4-MMC are calculated at 1606, 1562, near 1500, and 1400 cm^{-1} (exp.: 1605, 1569, 1492, and 1412 cm^{-1}, respectively). In contrast to 2-MMC, the band of symmetric C=C vibrations near 1600 cm^{-1} has a strong IR intensity in agreement with the experiment (Figure 8, Table 4).

Asymmetric C=C vibrations of the Kekule type produce weak IR bands in the observed spectra of 2- and 4-MMC compounds at 1300 cm^{-1} (calc.: 1293 and 1294 cm^{-1} in dimers 1 and 2 of 2-MMC, respectively; calc.: 1310 cm^{-1}, exp.: 1295 cm^{-1} in 4-MMC, Tables 3 and 4).

The asymmetric deformations of methyl groups (CH_3 def., as.) in the IR spectrum of 2-MMC are calculated in the frequency region 1471–1415 cm^{-1}; symmetric deformations of a methyl group – in the range 1405–1372 cm^{-1} (Tables S3, S4 in SI). These vibrations are mixed with wagging and twisting deformation vibrations of NH_2 groups. In the experimental spectrum, these CH_3 (def., as.) vibrations produce a band of 1459 cm^{-1} of middle intensity and a weak band of 1430 cm^{-1} (calc.: 1450, 1427 cm^{-1}, respectively, in dimer 1 and 1452, 1430 cm^{-1} in dimer 2). The symmetric CH_3 (def., s.) vibrations produce a band 1380 cm^{-1} (calc.: 1376 and 1388 cm^{-1} in dimers 1 and 2, respectively, Figure 7). Corresponding methyl deformation (CH_3 def., as.) bands of 4-MMC dimer in the IR spectrum are observed at 1457, and 1467 cm^{-1} (left shoulder on a strong band 1457 cm^{-1}), and their symmetric counterparts (CH_3 def., s.) vibrations produce the bands 1412 and 1384 cm^{-1} of middle intensity (Figure 8, Table 4). These IR manifestations of methyl groups provide an important analytical remedy because of their different positions in the two studied drugs. Detailed assignment of all CH_3 vibrational modes could help to distinguish between both isomers.

Wagging deformation vibrations of the NH_2 group (NH_2 wag.) contribute to the experimental bands 1459, 1430 cm^{-1} of the 2-MMC compound and 1467, 1457, 1412 cm^{-1} IR bands of 4-MMC. The twisting deformations (NH_2 twist.) contribute to the observed bands 1380, 1336, 1300 cm^{-1} and 1457, 1384, 1347, 1295 cm^{-1} of 2- and 4-MMC, respectively. The rocking vibrations of the amino group (NH_2 rock.) produce the experimental IR bands 1166, 1137, 973 cm^{-1} and 1201, 1189, 1166, 889 cm^{-1} for 2- and 4-MMC compounds, respectively (Figures 7 and 8, Tables S3–S5 in SI).

Vibrations of single bonds C–C and C–N are calculated in the range 1248–798 cm^{-1}. In the experimental IR spectrum of the 4-MMC compound, they correspond to the strong bands

at 1248 cm^{-1} (calc.: a split band with maxima at 1256 and 1238 cm^{-1}), 1096 (calc.: 1098 cm^{-1}), 1008 cm^{-1} (calc.: 1006 cm^{-1}), 976 cm^{-1} (calc.: 978 cm^{-1}) and several weak bands at 1215, 1166, 1050, 854 and 802 cm^{-1} (Figure 8). They are accompanied by deformation vibrations of methyl groups and CH bending vibrations. In the observed spectrum of 2-MMC compound C–C and C–N skeletal vibrations correspond to the moderate and weak bands at 1246, 1200, 1095, 1030, 1007, 973, and 845 cm^{-1} (Figure 7, Tables S3, S4 in SI).The late band at845 cm^{-1} is responsible only for the C–N stretching vibration.

The aromatic in-plane CCH deformation vibrations (CCH_{Ar} bend) are predicted in 1276–1060 cm^{-1} (Tables S3–S5 in SI) with a very weak IR absorption. Thus, they have no large analytical importance, and their discussion is given in the SI.

The low experimental intensity IR band of 4-MMC at 510 cm^{-1} (Figure 8, curve 2) was assigned to libration movement of the salt fragments NH_2^+ relative Cl atoms (Table 4, calc.: 512 and 507 cm^{-1} for molecules 1 and 2 in dimer). There is no vibration of this type in the 2-MMC dimers in this frequency range. The dimeric simulation of crystal structure for both drags many other interesting differences in the low-frequency vibrations, but this is outside the scope of IR spectra and will be the subject of the Raman scattering study. All other absorption bands are listed in Tables S3–S5 in SI.

4. Conclusions

In the course of the systematic IR study of the methcathinone drug series, we present in this paper the DFT modeling calculations of crystalline 2- and 4-methyl methcathinone (2-MMC and 4-MMC) hydrochlorides IR spectra, which strongly depend on the crystal packing details and, in particular – on the character of the methcathinone molecules interact with the hydrochloride moiety. The task of such DFT simulations is proved to be very difficult and requires modeling a great number of molecular dimers. The DFT geometry optimization was initiated with the experimental crystal structure derived from the X-ray analysis, where the methcathinone dimer structure simulated the elementary cell. Thus, it leads to HCl coordination on the amino group instead of binding to the C=O group, which was obtained in the case of one methcathinone molecule. The DFT optimized structures of the dimers $(2\text{-MMC}\cdot HCl)_2$ and $(4\text{-MMC}\cdot HCl)_2$ explain the IR observed spectra. The Hirshfeld surfaces analysis of two simulated crystalline methyl methcathinone hydrochlorides affords to analyze NH···Cl and CH···Cl intermolecular interactions and approves the formation of the NH_2^+–Cl^- salt fragment in both 2-MMC·HCl and 4-MMC·HCl crystals. Bader's "QTAIM" analysis of density gradients supported the correct nature of intermolecular interactions in the dimers in accord with the Hirshfeld surfaces for the whole crystal cells additionally.

Despite small discrepancies in the crystal structure parameters (in particular - overestimation of the carbonyl bond length, which leads to the IR band shift for the C=O valence vibration), the applied DFT method permits us to predict the main peculiarities of the simulated dimers structures and IR spectra of two cathinone hydrochlorides. The proper HCl coordination on NH-groups upon the formation of the dimer provides a correct description of IR spectra for both studied compounds, including the high-frequency and fingerprint regions.

This pure theoretical study of crystalline structure and IR spectra of methcathinone hydrochloride drug compounds provides a complete assignment to a certain category of psychotropic substances. Many structural features are connected with their IR spectroscopic manifestations, which can be used in forensic studies. Interpretation of the complicated nature

of the IR bands associated with the vibration of the salt $NH_2^+Cl^-$ moiety is an important achievement of the density functional theory.

Funding

This research received no external funding.

Acknowledgments

This study was supported by the Ministry of Education and Science of Ukraine (projects no. 0121U107533).

Conflicts of Interest

The authors declare no conflict of interest.

References

1. Islam, M.W.; Tariq, M.; Ageel, A.M.; El-Feraly, F.S.; Al-Meshal, I.A.; Ashraf, I. An evaluation of the male reproductive toxicity of cathinone. *Toxicology* **1990**, *60*, 223–234, https://doi.org/10.1016/0300-483x(90)90145-7.
2. Valente, M.J.; de Pinho, P.G.; de Lourdes Bastos, M.; Carvalho, F.; Carvalho, M. Khat and synthetic cathinones: a review. *Arch. Toxicol* **2014**, *88*, 15–45, https://doi.org/10.1007/s00204-013-1163-9.
3. Simmler, L.D.; Buser, T.A.; Donzelli, M.; Schramm, Y.; Dieu, L.-H.; Huwyler, J.; Chaboz, S.; Hoener, M.C.; Liechti, M.E. Pharmacological characterization of designer cathinones in vitro. *British Journal of Pharmacology* **2013**, *168*, 458–470, https://doi.org/10.1111/j.1476-5381.2012.02145.x.
4. Baumann, M.H.; Partilla, J.S.; Lehner, K.R. Psychoactive "bath Salts": Not So Soothing. *Eur. J. Pharmacol* **2013**, *698*, 1–5, https://doi.org/10.1016/j.ejphar.2012.11.020.
5. Glennon, R.A.; Dukat, M. Structure-activity relationship of synthetic cathinones. *Curr. Top. Behav. Neurosci* **2016**, *32*, 19–47, https://doi.org/10.1007/7854_2016_41.
6. Yadav-Samudrala, B.J.; Eltit, J.M.; Glennon, R.A. Synthetic Cathinone Analogues Structurally Related to the Central Stimulant Methylphenidate as Dopamine Reuptake Inhibitors. *ACS Chem. Neurosci* **2019**, *10*, 4043–4050, https://doi.org/10.1021/acschemneuro.9b00284.
7. Nadal-Gratacós, N.; Alberto-Silva, A.S.;Rodríguez-Soler, M.; Urquizu, E.; Espinosa-Velasco, M.; Jäntsch, K.; Holy, M.;Batllori, X.; Berzosa, X.; Pubill, D.;Camarasa, J.; Sitte, H.H.; Escubedo, E.; López-Arnau, R. Structure–Activity Relationship of Novel Second-Generation Synthetic Cathinones: Mechanism of Action, Locomotion, Reward, and Immediate-Early Genes *Front. Pharmacol*. **2021**, https://doi.org/10.3389/fphar.2021.749429.
8. Moreno, A.Y.; Mayorov, A.V.; Janda K.D. Impact of Distinct Chemical Structures for the Development of a Methamphetamine Vaccine. *J. Am. Chem. Soc.* **2011**, *133*, 6587–6595, https://doi.org/10.1021/ja108807j.
9. Soares, J.; Costa, V.M.; Bastos, M.deL.; Carvalho, F.; Capela, J.P. An updated review on synthetic cathinones. *Arch. Toxicol.* **2021**, *95*, 2895–2940, https://doi.org/10.1007/s00204-021-03083-3.
10. Bolcato, V.; Carelli, C.; Radogna, A.; Freni, F.; Moretti, M.; Morini, L. New Synthetic Cathinones and Phenylethylamine Derivatives Analysis in Hair: A Review. *Molecules* **2021**, *26*, https://doi.org/10.3390/molecules26206143.
11. Lucchetta, R.C.; Riveros, B.S.; Pontarolo, R.; Radominski, R.B.; Otuki, M.F.; Fernandez-Llimos, F.; Correr, C.J. Systematic review and meta-analysis of the efficacy and safety of amfepramone and mazindol as a monotherapy for the treatment of obese or overweight patients. *Clinics* **2017**, *72*, 317–324, https://doi.org/10.6061/clinics/2017(05)10.
12. Soto-Molina, H.; Pizarro-Castellanos, M.; Rosado-Pérez, J.; Rizzoli-Córdoba, A.; Lara-Padilla, E.; Fernández del Valle- Laisequilla, C.; Reyes-García, J.G. Six-month efficacy and safety of amfepramone in obese Mexican patients: a double-blinded, randomized, controlled trial. *Int. J. Clin. Pharmacol. Ther*. **2015**, *53*, 541–549.
13. Patel, K.; Allen, S.; Haque, M.N.; Angelescu, I.; Baumeister, D.; Tracy, D.K. Bupropion: a systematic review and meta-analysis of effectiveness as an antidepressant. *Ther. Adv. Psychopharmacol*. **2016**, *6*, 99–144, https://doi.org/10.1177/2045125316629071.
14. González-Urbieta, I.; Jafferany, M.; Torales, J. Bupropion in dermatology: A brief update. *Dermatologic Therapy* **2021**, *34*, https://doi.org/10.1111/dth.14303.

15. Kolaczynska, K.E.; Thomann, J.; Hoener, M.C.; Liechti, M.E. The Pharmacological Profile of Second Generation Pyrovalerone Cathinones and Related Cathinone Derivative. *Int. J. Mol. Sci.* **2021**, *22*, 8277–8293, https://doi.org/10.3390/ijms22158277.
16. Souders, C.L.; Davis, R.H.; Qing, H.; Liang, X.; Febo, M.; Martyniuk, C.J. The psychoactive cathinone derivative pyrovalerone alters locomotor activity and decreases dopamine receptor expression in zebrafish (Danio rerio). *Brain Behav*. **2019**, *9*, https://doi.org/10.1002/brb3.1420.
17. Sørensen, L.K. Determination of cathinones and related ephedrines in forensic whole-blood samples by liquid-chromatography–electrospray tandem mass spectrometry. *Journal of Chromatography B* **2011**, *879*, 727–736, https://doi.org/10.1016/j.jchromb.2011.02.010.
18. Schmid, M.G.; Hägele, J.S. Separation of enantiomers and positional isomers of novel psychoactive substances in solid samples by chromatographic and electrophoretic techniques – A selective review. *J. Chromatogr. A* **2020**, *1624*, https://doi.org/10.1016/j.chroma.2020.461256.
19. Trinklein, T.J.; Thapa, M.; Lanphere, L.A.; Frost, J.A.; Koresch, S.M.; Aldstadt III, J.H. Sequential injection analysis coupled to on-line benchtop proton NMR: Method development and application to the determination of synthetic cathinones in seized drug samples. *Talanta* **2021**, *231*, https://doi.org/10.1016/j.talanta.2021.122355.
20. Loganathan, D.; Yi, R.; Patel, B.; Zhang, J.; Kong, N. A sensitive HPLC-MS/MS method for the detection, resolution and quantitation of cathinone enantiomers in horse blood plasma and urine. *Anal. Bioanal. Chem.* **2021**, *413*, 2147–2161, https://doi.org/10.1007/s00216-021-03182-1.
21. McNeill, L.; Pearson, C.; Megson, D.; Norrey, J.; Watson, D.; Ashworth, D.; Linton, P.E.; Sutcliffe, O.B.; Shaw, K.J. Origami chips: Development and validation of a paper-based Lab-on-a-Chip device for the rapid and cost-effective detection of 4-methylmethcathinone (mephedrone) and its metabolite, 4-methylephedrine in urine. *Forensic Chem.* **2021**, *22*, https://doi.org/10.1016/j.forc.2020.100293.
22. Faivre, D. Introduction to Standard Spectroscopic Methods: XRD, IR/Raman, and Mössbauer. *Wiley* **2016**, https://doi.org/10.1002/9783527691395.ch13.
23. Morin, P. Separation of chiral pharmaceutical drugs by chromatographic and electrophoretic techniques. *Ann. Pharm. Fr.* **2009**, *67*, 241–250, https://doi.org/10.1016/j.pharma.2009.03.008.
24. Silva, B.; Fernandes, C.; de Pinho, P.G.; Remião, F. Chiral Resolution and Enantioselectivity of Synthetic Cathinones: A Brief Review. *J. Anal. Toxicol*. **2017**, *42*, 17–24, https://doi.org/10.1093/jat/bkx074.
25. Hägele, J.S.; Basrak, M.; Schmid, M.G. Enantioselective separation of Novel Psychoactive Substances using a Lux® AMP 3 µm column and HPLC-UV. *J. Pharm. Biomed. Anal*. **2020**, *179*, https://doi.org/10.1016/j.jpba.2019.112967.
26. Spálovská, D.; Paškan, M.; Jurásek, B.; Kuchař, M.; Kohout, M.; Setnička, V. Structural spectroscopic study of enantiomerically pure synthetic cathinones and their major metabolites. *New J. Chem.* **2021**, *45*, 850–860, https://doi.org/10.1039/D0NJ05065B.
27. Daeid, N.N.; Savage, K.A.; Ramsay, D.; Holland, C.; Sutcliffe, O.B. Development of gas chromatography–mass spectrometry (GC–MS) and other rapid screening methods for the analysis of 16 'legal high' cathinone derivatives. *Science & Justice* **2014**, *54*, 22–31, https://doi.org/10.1016/j.scijus.2013.08.004.
28. Vujović, M.; Ragavendran, V.; Arsić, B.; Kostić, E.; Mladenović, M. DFT calculations as an efficient tool for prediction of Raman and infra-red spectra and activities of newly synthesized cathinones. *Open Chem.* **2020**, *18*, 185–195, https://doi.org/10.1515/chem-2020-0021.
29. Hui, C. Identification of cathinone drug by $B_{24}N_{24}$ nanocage: a DFT/TDDFT investigation. *Mol. Phys.* **2021**, *120*, https://doi.org/10.1080/00268976.2021.2009927.
30. Xu, W.; Cao, H.; Chen, H.; Yang, Y.; Sarkar, A. Sensing the cathinone drug concentration in the human body by using zinc oxide nanostructures: a DFT study. *Struct. Chem.* **2021**, *32*, 63–68, https://doi.org/10.1007/s11224-020-01611-y.
31. Cao, Y.; Farouk, N.; Issakhov, A.; Anqi, A.E.; Derakhshandeh, M. A DFT study on the detection of cathinone drug on the Au-decorated BC_3 nanosheet. *Phys. E: Low-Dimens. Syst. Nanostructures* **2021**, *134*, https://doi.org/10.1016/j.physe.2021.114931.
32. Rodrigues, C.H.P.; Leite, V.B.P.; Bruni, A.T. Can NMR spectroscopy discriminate between NPS amphetamines and cathinones? An evaluation by in silico studies and chemometrics. *Chemometr. Intell. Lab. Syst.* **2021**, *210*, https://doi.org/10.1016/j.chemolab.2021.104265.
33. Minaeva, V.A.; Karaush-Karmazin, N.N.; Panchenko, A.A.; Heleveria, D.N.; Minaev, B.F. Hirshfeld surfaces analysis and DFT study of the structure and IR spectrum of N-ethyl-2-amino-1-(4-chlorophenyl)propan-1-one (4-CEC) hydrochloride. *Comput. Theor. Chem.* **2021**, *1205*, https://doi.org/10.1016/j.comptc.2021.113455.
34. Glennon, R.A. Bath salts, mephedrone, and methylenedioxypyrovalerone as emerging illicit drugs that will need targeted therapeutic intervention. *Advances in Pharmacology* **2014**, *69*, 581-620, https://doi.org/10.1016/B978-0-12-420118-7.00015-9.
35. Maheux, C.R.; Copeland, C.R. Characterization of Three Methcathinone Analogs: 4-Methylmethcathinone, Methylone, and bk-MBDB. *Microgram Journal* **2010**, *7*, 42–49.
36. Camilleri, A.; Johnston, M. R.; Brennan, M.; Davis, S.; Caldicott, D.G.E. Chemical analysis of four capsules containing the controlled substance analogues 4-methylmethcathinone, 2-fluoromethamphetamine, alpha-

phthalimidopropiophenoneand *N*-ethylcathinone. *Forensic Sci. Int.* **2010**, *197*, 59–66, https://doi.org/10.1016/j.forsciint.2009.12.048.
37. Power, J.D.; McGlynn, P.; Clarke, K.; McDermott, S.D.; Kavanagh, P.; O'Brien, J. The analysis of substituted cathinones. Part 1: chemical analysis of 2-, 3- and 4-methylmethcathinone. *Forensic Sci. Int*. **2011**, *212*, 6–12, https://doi.org/10.1016/j.forsciint.2011.04.020.
38. Schifano, F.; Albanese, A.; Fergus, S.; Stair, J. L.; Deluca, P.; Corazza, O.; Davey, Z.; Corkery, J.; Siemann, H.; Scherbaum, N.; Farre', M.; Torrens, M.; Demetrovics, Z.; Ghodse, A.H. Mephedrone (4-methylmethcathinone; 'meow meow'): chemical, pharmacological and clinical issues. *Psychopharmacology* **2011**, *214*, 593–602, https://doi.org/10.1007/s00213-010-2070-x.
39. Kuś, P.; Hellwig, H.; Kusz, J.; Książek, M.; Rojkiewicz, M.; Sochanik, A. Crystal structures and other properties of ephedrone (methcathinone) hydrochloride, N-acetylephedrineand N-acetylephedrone. *Forensic Toxicol*. **2019**, *37*, 224–230, https://doi.org/10.1007/s11419-018-0436-7.
40. Nycz, J.E.; Malecki, G.; Zawiazalec, M.; Pazdziorek, T. X-ray structures and computational studies of several cathinones. *J. Mol. Struct.* **2011**, *1002*, 10–18, https://doi.org/10.1016/j.molstruc.2011.06.030.
41. Nycz, J.E.; Pazdziorek, T.; Malecki, G.; Szala, M. Identification and derivatization of selected cathinones by spectroscopic studies. *Forensic Sci. Int*. **2016**, *266*, 416–426, https://doi.org/10.1016/j.forsciint.2016.06.034.
42. Minaeva, V.; Minaev, B.; Panchenko, A.; Pasychnik, V. Computational study of IR, Raman and NMR spectra of 4-methylmethcathinone drug. *J. Mol. Model.* **2021**, *27*, https://doi.org/10.1007/s00894-020-04658-0.
43. Becke, A.D. Density-functional thermochemistry. III. The role of exact exchange. *J. Chem. Phys.* **1993**, *98*, 5648–5652, https://doi.org/10.1063/1.464913.
44. Stewart, J.J.P. Optimization of parameters for semi-empiricalmethods I. Method. *J. Comput. Chem.* **1989**, *10*, 209–220, https://doi.org/10.1002/jcc.540100208.
45. Stewart, J.J.P. Optimization of parameters for semi-empiricalmethods IV: extension of MNDO, AM1, and PM3 to more maingroup elements. *J. Mol. Model.* **2004**, *10*, 155–164, https://doi.org/10.1007/s00894-004-0183-z.
46. Spackman, P.R.; Turner, M.J.; McKinnon, J.J.; Wolff, S.K.; Grimwood, D.J.; Jayatilaka, D.; Spackman, M.A. CrystalExplorer: a program for Hirshfeld surface analysis, visualization and quantitative analysis of molecular crystals. *J. Appl. Cryst.* **2021**, *54*, 1006–1011, https://doi.org/10.1107/S1600576721002910.
47. Hirshfeld, F.L. Bonded-Atom Fragments for Describing Molecular Charge Densities. *Theoret. Claim. Acta (Berl.)* **1977**, *44*, 129–138, https://doi.org/10.1007/BF00549096.
48. Spackman, M.A.; Jayatilakaa, D. Hirshfeld surface analysis. *Cryst. Eng. Comm.* **2009**, *11*, 19–32, https://doi.org/10.1039/B818330A.
49. Becke, A.D. Perspective: Fifty years of density-functional theory in chemical physics. *J. Chem. Phys.* **2014**, *140*, https://doi.org/10.1063/1.4869598.
50. Mardirossian, N.; Head-Gordon, M. Thirty years of density functional theory in computational chemistry: an overview and extensive assessment of 200 density functional. *Mol. Phys.* **2017**, *115*, 1–58, https://doi.org/10.1080/00268976.2017.1333644.
51. Lee, C.; Yang, W.; Parr, R.G. Development of the Colle-Salvetti correlation-energy formula into a functional of the electron density. *Phys. Rev. B* **1988**, *37*, 785–789, https://doi.org/10.1103/PhysRevB.37.785.
52. Francl, M.M.; Petro, W.J.; Hehre, W.J.; Binkley, J.S.; Gordon, M.S.; DeFrees, D.J.; Pople, J.A. Self-consistent molecular orbital methods. XXIII. A polarization-type basis set for second-row elements. *J. Chem. Phys*. **1982**, *77*, 3654–3666, https://doi.org/10.1063/1.444267.
53. Frisch, M.J.; Trucks, G.W.; Schlegel, H.B.; Scuseria, G.E.; Robb, M.A.; Cheeseman, J.R.; Scalmani, G.; Barone, V.; Petersson, G.A.; Nakatsuji, H.; Li, X.; Caricato, M.; Marenich, A.V.; Bloino, J.; Janesko, B.G.; Gomperts, R.; Mennucci, B.; Hratchian, H.P.; Ortiz, J.V.; Izmaylov, A.F.; Sonnenberg, J.L.; Williams-Young, D.; Ding, F.; Lipparini, F.; Egidi, F.; Goings, J.; Peng, B.; Petrone, A.; Henderson, T.; Ranasinghe, D.; Zakrzewski, V.G.; Gao, J.; Rega, N.; Zheng, G.; Liang, W.; Hada, M.; Ehara, M.; Toyota, K.; Fukuda, R.; Hasegawa, J.; Ishida, M.; Nakajima, T.; Honda, Y.; Kitao, O.; Nakai, H.; Vreven, T.; Throssell, K.; Montgomery Jr, J.A.; Peralta, J.E.; Ogliaro, F.; Bearpark, M.J.; Heyd, J.J.; Brothers, E.N.; Kudin, K.N.; Staroverov, V.N.; Keith, T.A.; Kobayashi, R.; Normand, J.; Raghavachari, K.; Rendell, A.P.; Burant, J.C.; Iyengar, S.S.; Tomasi, J.; Cossi, M.; Millam, J.M.; Klene, M.; Adamo, C.; Cammi, R.; Ochterski, J.W.; Martin, R.L.; Morokuma, K.; Farkas, O.; Foresman, J.B.; Fox, D.J. Gaussian 16, Revision A.03, Gaussian, Inc., Wallingford, CT **2016**.
54. Scott, A.P.; Radom, L. Harmonic Vibrational Frequencies: An Evaluation of Hartree−Fock, Møller−Plesset, Quadratic Configuration Interaction, Density Functional Theory, and Semiempirical Scale Factors. *J. Phys. Chem.* **1996**, *100*, 16502–16513, https://doi.org/10.1021/jp960976r.
55. Karaush, N.N.; Minaev, B.F.; Baryshnikov, G.V.; Minaeva, V.A. A comparative study of the electronic structure and spectra of tetraoxa[8]circulene and octathio[8]circulene. *Opt. Spectrosc*. **2014**, *116*, 33–46, https://doi.org/10.1134/S0030400X13120084.
56. Minaeva, V.A.; Karaush, N.N.; Minaev, B.F.; Baryshnikov, G.V.; Chen, F.; Tanaka, T.; Osuka, A. Comparative study of the structural and spectral properties of tetraaza- and tetraoxaannelated tetracirculenes. *Opt. Spectrosc*. **2017**, *122*, 523–540, https://doi.org/10.1134/S0030400X17030134.

57. Minaeva, V.A.; Baryshnikov, G.V.; Minaev, B.F.; Karaush, N.N.; Xiong, X.-D.; Li, M.-D.; Phillips, D.L.; Wong, H.N.C. Structure and spectroscopic characterization of tetrathia- and tetraselena[8]circulenes as a new class of polyaromatic heterocycles. *Spectrochim. Acta, Part A* **2015**, *151*, 247–261, https://doi.org/10.1016/j.saa.2015.06.020.
58. Karaush, N.N.; Minaeva, V.A.; Baryshnikov, G.V.; Minaev, B.F.; Ågren, H. Identification of tautomeric intermediates of a novel thiazolylazonaphthol dye – A density functional theory study. *Spectrochim. Acta Part A* **2018**, *203*, 324–332, https://doi.org/10.1016/j.saa.2018.05.096.
59. Gorelsky, S.I. SWizard program, University of Ottawa, Ottawa, Canada **2013**, http://www.sg-chem.net.
60. Dennington, R.; Keith, T.A.; Millam, J.M. GaussView, Version 6, Semichem Inc., 235 Shawnee Mission, KS **2016**.
61. Bader, R.F.W. *Atoms in Molecules. A Quantum Theory*. Clarendon Press, Oxford **1990**.
62. Keith T.A. AIMAll (Version 10.07.25), TK Gristmill Software, Overland ParkKS, USA, **2010**, www.aim.tkgristmill.com.
63. Espinosa, E.; Molins, E.; Lecomte, C. Hydrogen bond strengths revealed by topological analyses of experimentally observed electron densities. *Chem. Phys. Lett.* **1998**, *285*, 170–173, https://doi.org/10.1016/S0009-2614(98)00036-0.
64. Espinosa, E.; Alkorta, I.; Rozas, I.; Elguero, J.; Molins, E. About the evaluation of the local kinetic, potential and total energy densities in closed-shell interactions. *Chem. Phys. Lett.* **2001**, *336*, 457–461, https://doi.org/10.1016/S0009-2614(01)00178-6.
65. Karaush, N.N.; Baryshnikov, G.V.; Minaeva, V.A.; Minaev, B.F. A DFT and QTAIM study of the novel d-block metal complexes with tetraoxa[8]circulene-based ligands. *New J. Chem.* **2015**, *39*, 7815–7821, https://doi.org/10.1039/C5NJ01255D.
66. Socrates, G. Infrared Raman Characteristic Group Frequencies – Tables and Charts, 3rd ed. *J. Wiley&Sons, Chichester* **2001**, https://doi.org/10.1021/ja0153520.

Supplementary Information

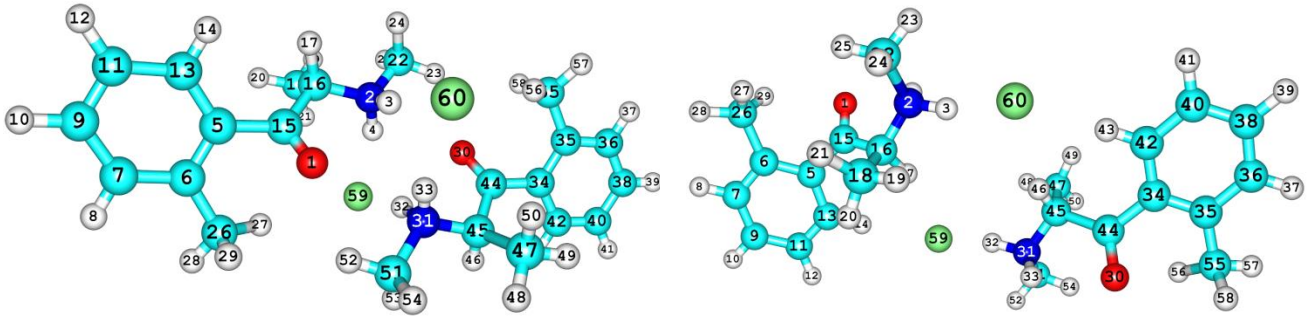

DIMER 1 (2-MMC) DIMER 2 (2-MMC)

a

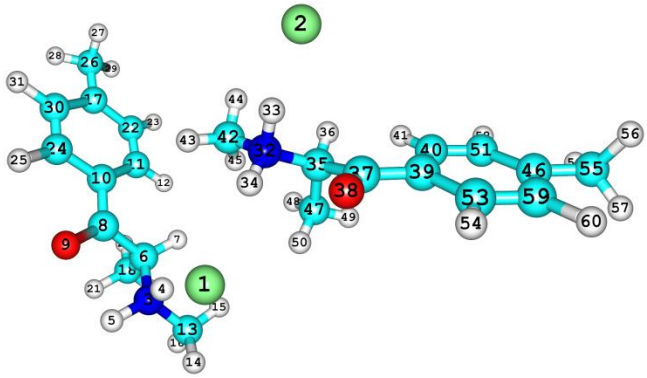

DIMER (4-MMC)

b

Figure S1. The structures of the corresponding dimers selected from crystals of 2-MMC (*a*) and 4-MMC (*b*) optimized at the B3LYP/6-31G(d,p) theory level. Oxygen atoms are in red; Chlorine atoms are in turquoise; Nitrogen atoms are in blue.

Table S1. Selected bond lengths (Å) and angles (deg) for dimer 1 and dimer 2 of 2-methylmethcathinone hydrochloride.

Structural parameters	Dimer1	Dimer2	Bond lengths and angles, exp., [33]
	Bond lengths and angles, theor.	Bond lengths and angles, theor.	
O1–C15, O30–C44	1.218	1.227	1.213
C5–C15, C34–C44	1.494	1.487	1.492
C15–C16, C44–C45	1.549	1.545	1.525
C16–N2, C45–N31	1.497	1.506	1.487
N2–H3Cl, N31–H32Cl	0.969	0.985	0.891
N2–H4, N31–H33	0.948	0.924	0.890
N2–C22H$_3$, N31–C51H$_3$	1.492	1.492	1.484
C16–H17, C45–H46	1.097	1.102	0.980
C16–C18H$_3$, C45–C47H$_3$	1.535	1.530	1.518
C6$_{Ar}$–C26H$_3$, C35$_{Ar}$–C55H$_3$	1.510	1.511	1.501
C5–C6, C34–C35	1.416	1.418	1.398
C6–C7, C35–C36	1.401	1.398	1.393
C7–C9, C36–C38	1.394	1.396	1.384
C9–C11, C38–C40	1.395	1.393	1.372
C11–C13, C40–C42	1.391	1.393	1.381
C5–C13, C34–C42	1.405	1.405	1.389
H3–Cl 60, H32–Cl 59	2.023	2.023	2.272
H3N2H4 H32N31H33	107.42 107.45	109.31 108.94	107.58
N2C16C15C5 N31C45C44C34	–173.68 172.05	–173.53 172.05	–172.05(**1**) 172.05(**2**)
C6C5C15C16	141.39	141.26	139.72(**1**)

Structural parameters	Dimer1	Dimer2	Bond lengths and angles, exp., [33]
	Bond lengths and angles, theor.	Bond lengths and angles, theor.	
C35C34C44C45	–137.88	–141.42	–139.72(**2**)
C6C5C15O1	–39.74	–39.74	–39.74(**1**)
C35C34C44O30	39.74	39.74	39.74(**2**)
C5C15C16C18	–51.42	–48.42	–48.31(**1**)
C34C44C45C47	49.92	47.07	48.31(**2**)
C26C6C5C15	0.15	0.15	0.15(**1**)
C55C35C34C44	–0.15	–0.15	–0.15 (**2**)

Table S2. Selected bond lengths (Å) and angles (deg) for the dimer calculated at the B3LYP/6-31G(d,p) level.

Molecule 1		Molecule 2		Bond lengths and angles, exp. [32]
Structural parameters	Bond lengths and angles, theor.	Structural parameters	Bond lengths and angles, theor.	
O9–C8	1.227	O38–C37	1.219	1.228
C22–C11	1.394	C51–C40	1.394	1.400
C11–C10	1.404	C40–C39	1.402	1.395
C22–C17	1.400	C51–C46	1.400	1.370
$C17_{Ar}$–$C26H_3$	1.509	$C46._{Ar}$–$C55H_3$	1.509	1.526
C17–C30	1.405	C46–C59	1.405	1.378
C24–C30	1.387	C53–C59	1.387	1.387
C10–C24	1.406	C39–C53	1.406	1.396
C10–C8	1.482	C39–C37	1.491	1.492
C6–N3	1.501	C35–N32	1,490	1.489
C6–H7	1.091	C35–H36	1.092	0.980
N3–C13	1.491	N32–C42	1.485	1.476
N3–H4Cl1	0.962	N32–H33	0.966	0.899
N3–H5	0.923	Cl132–H34	0.940	0.900
NH4–Cl1	1.992	NH33–Cl 2	1.993	2.182
C6H7–Cl1	3.757			3.758
NH34(**2**)···Cl1(**1**)	2.105			2.226
C10C24C30	120.42	C39C53C59	120.55	119.25
C24C30C17	120.84	C53C59C46	121.09	121.39
C30C17C22	118.39	C59C46C51	118.15	119.28
C17C22C11	121.35	C46C51C40	121.10	121.08
C22C11C10	119.76	C51C40C39	120.48	119.20
H4N3H5	107.53	H33N32H34	104.06	107.53
C13N3C6C18	66.46	C42N32C35C47	–66.46	66.46 (**1**) –66.46 (**2**)
N3C6C8C10	162.47	N32C35C37C39	–162.47	162.46 (**1**) –162.46 (**2**)
C8C6N3C13	–176.18	C37C35N32C42	173.10	–169.74 (**1**) 169.74 (**2**)
O9C8C6N3	–22.66	O38C37C35N3	23.84	–23.10(**1**) 23.10(**2**)

Table S3. Calculated frequencies, IR intensities, corresponding experimental date, and assignment of vibrational modes for the dimer 1 of 2-methylmethcathinone hydrochloride determined at the B3LYP/6-31G(d,p) level.

Mode	DFT freq. calc.	Exp. [29]	I_{IR}	Assignment
ν_{174}	3039		2	$C22H_3$ str., as., **1**
ν_{173}	3038		1	$C51H_3$ str., as., **2**
ν_{172}	3037	3024	18	C–H_{Ar} str., iph., **1**
ν_{171}	3037	3024	23	C–H_{Ar} str., iph., **2**
ν_{170}	3024	3024	25	C–H_{Ar} str., ooph., **1**
ν_{169}	3024	3024	24	C–H_{Ar} str., ooph., **2**
ν_{168}	3016		4	$C51H_3$ str., as., **2**
ν_{167}	3016		5	$C22H_3$ str., as., **1**
ν_{166}	3015		2	C–H_{Ar} str., ooph., **1**
ν_{165}	3014		2	C–H_{Ar} str., ooph., **2**

Mode	DFT freq. calc.	Exp. [29]	I_{IR}	Assignment
ν_{164}	3009		6	C–H_{Ar} str., ooph., **1**
ν_{163}	3008		6	C–H_{Ar} str., ooph., **2**
ν_{162}	2996	2984	10	$C47H_3$ str., as., **2**
ν_{161}	2995	2984	9	$C18H_3$ str., as., **1**
ν_{160}	2972	2984	18	$C18H_3$ str., as., **1**, $C47H_3$ str., as., **2**
ν_{159}	2972		3	$C18H_3$ str., as., **1**, $C47H_3$ str., as., **2**
ν_{158}	2961	2959	22	$C55H_{3\,Ar}$ str., as., **2**
ν_{157}	2960	2959	19	$C26H_{3\,Ar}$ str., as., **1**
ν_{156}	2945		12	$C26H_{3\,Ar}$ str., as., **1**
ν_{155}	2944		13	$C55H_{3\,Ar}$ str., as., **2**
ν_{154}	2933	2920	110	$C22H_3$ str., s., **1**, N–H4 (**1**)···Cl 59 (**2**) str., $C51H_3$ str., s., **2**, N–H33 (**2**)···Cl 60 (**1**) str., ooph.
ν_{153}	2933		0.3	$C22H_3$ str., s., **1**, N–H4 (**1**)···Cl 59 (**2**) str., $C51H_3$ str., s., **2**, N–H33 (**2**)···Cl 60 (**1**) str., iph.
ν_{152}	2899	2895	51	$C18H_3$ str., s., **1**, $C47H_3$ str., s., **2**, ooph.
ν_{151}	2899		0.1	$C18H_3$ str., s., **1**, $C47H_3$ str., s., **2**, iph.
ν_{150}	2882		35	$C26H_{3\,Ar}$ str., s., **1**
ν_{149}	2882		12	$C55H_{3\,Ar}$ str., s., **2**
ν_{148}	2774	2742	280	N2–H4 (**1**)···Cl 59 (**2**) str., C16–H str., **1**, N31–H33 (**2**) ···Cl 60 (**1**) str., C45–H str., **2**, iph.
ν_{147}	2766		2	N2–H4 (**1**)···Cl 59 (**2**) str., C16–H str., s., **1**, N31–H33 (**2**)···Cl 60 (**1**) str., **2**, ooph.
ν_{146}	2753	2742	256	N2–H4 (**1**)···Cl 59 (**2**) str., C16–H str., **1**, N31–H33 (**2**)···Cl 60 (**1**) str., C45–H str., **2**, ooph.
ν_{145}	2747		2	N2–H4 (**1**)···Cl 59 (**2**) str., C16–H str., **1**, N31–H33 (**2**)···Cl 60 (**1**) str., C45–H str., **2**, iph.
ν_{144}	2458	2451	805	N2–H3–Cl 60 str., **1**, N31–H32–Cl 59 str., **2**, ooph., N–H4 (**1**)···Cl 59 (**2**) str., **1**, N–H33 (**2**)···Cl 60 (**1**) str., **2**
ν_{143}	2419	2364	4	N2–H3–Cl 60 str., **1**, N31–H32–Cl 59 str., **2**, iph., N–H4 (**1**)···Cl 59 (**2**) str., **1**, N–H33 (**2**)···Cl 60 (**1**) str., **2**
ν_{142}	1714	1696	272	C=O str., NH_2 scis., **1**, **2**, ooph.
ν_{141}	1712	1696	113	C=O str., NH_2 scis., **1**, **2**, iph.
ν_{140}	1621	–	0.004	NH_2 scis., **1**, **2**, iph.
ν_{139}	1591	1600	17	C35=C36 and C40=C42 str., s., **2**
ν_{138}	1591	1600	12	C6=C7 and C11=C13 str., s., **1**
ν_{137}	1571	1572	35	NH_2 scis., **1**, **2**, ooph.
ν_{136}	1558	1550	9	C5=C6 and C9=C11 str., s., **1**
ν_{135}	1558	1550	52	C38=C40 and C34=C35 str., s., **2**
ν_{134}	1471	1489	23	$C18H_3$ def., as., $C22H_3$ def., as., $N3H_2$ wag., **1**, $C47H_3$ def., as., $C51H_3$ def., as., $N31H_2$ wag., **2**
ν_{133}	1470	–	0.2	$C18H_3$ def., as., $C22H_3$ def., as., C=C str., as., **1**, $C47H_3$ def., as., $C51H_3$ def., as., C=C str., as., **2**
ν_{132}	1467	–	9	CH_3 def., as., C=C str., as., C5–C15 str., **1**, CH_3 def., as., C=C str., as., C34–C44 str., **2**, ooph.
ν_{131}	1466	–	0.06	CH_3 def., as., C=C str., as., C5–C15 str., **1**, CH_3 def., as., C=C str., as., C34–C44 str., **2**, iph.
ν_{130}	1462	–	0.04	CH_3 def., as., NH_2 wag., **1**, **2**, iph.
ν_{129}	1462	1459	11	CH_3 def., as., NH_2 wag., **1**, **2**, ooph.
ν_{128}	1459	1459	122	CH_3 def., as., NH_2 wag., **1**, **2**, ooph.
ν_{127}	1457	–	5	CH_3 def., as., NH_2 twist., **1**, **2**
ν_{126}	1455	1459	30	$CH_{3\,Ar}$ def., as., NH_2 twist., **1**, **2**, $C47H_3$ def., as., **2**
ν_{125}	1453	–	2	CH_3 def., as., NH_2 twist., **1**, **2**
ν_{124}	1450	1459	93	$C18H_3$ def., as., $C22H_3$ def., as., $N2H_2$ wag., **1**, $C47H_3$ def., as., $C51H_3$ def., as., $N31H_2$ wag., **2**
ν_{123}	1448		0.1	$C18H_3$ def., as., $C22H_3$ def., as., $N2H_2$ wag., **1**, $C47H_3$ def., as., $C51H_3$ def., as., $N31H_2$ wag., **2**
ν_{122}	1441	1430	8	CH_{3Ar} def., as., **1**, **2**
ν_{121}	1440	1430	20	$CH_{3\,Ar}$ def., as., **1**, **2**
ν_{120}	1427	1417	95	$C18H_3$ def., as., $C22H_3$ def., as., $N2H_2$ wag., **1**, $C47H_3$ def., as., $C51H_3$ def., as., $N31H_2$ wag., **2**
ν_{119}	1419	1417	3	C=C str., as., $CH_{3\,Ar}$ def., as., **1**, **2**
ν_{118}	1418	1417	23	C=C str., as., $CH_{3\,Ar}$ def., as., **1**, **2**
ν_{117}	1415	–	0.02	$C18H_3$ def., as., $C22H_3$ def., as., $N2H_2$ wag., C16H bend., **1**, $C47H_3$ def., as., $C51H_3$ def., as., $N31H_2$ wag., C45H bend., **2**
ν_{116}	1405	1417	22	$C22H_3$ def., s., $N2H_2$ twist., C16H bend., **1**, $C51H_3$ def., s., $N31H_2$ twist., C45H bend., **2**

Mode	DFT freq. calc.	Exp. [29]	I_{IR}	Assignment
ν_{115}	1404	–	0.02	$C22H_3$ def., s., $N2H_2$ twist., **1**, $C51H_3$ def., s., $N31H_2$ twist., **2**
ν_{114}	1393		0.01	$C22H_3$ def., s., $N2H_2$ twist., C16H bend., **1**, $C51H_3$ def., s., $N31H_2$ twist., C45H bend., **2**
ν_{113}	1385	–	6	$C22H_3$ def., s., $N2H_2$ twist., C16H bend., **1**, $C51H_3$ def., s., $N31H_2$ twist., C45H bend., **2**
ν_{112}	1379		3	$C26H_3$ def., s., **1**
ν_{111}	1379		2	$C55H_3$ def., s., **2**
ν_{110}	1376		0.8	$C18H_3$ def., s., **1**, $C47H_3$ def., s., **2**, iph.
ν_{109}	1376	1380	42	$C18H_3$ def., s., $N2H_2$ twist., **1**, $C47H_3$ def., s.,$N31H_2$ twist., **2**, ooph.
ν_{108}	1308	1300	30	$N2H_2$ twist., C16H bend., $C22H_3$ rock., **1**, $N31H_2$ twist., C45H bend., $C51H_3$ rock., **2**, ooph.
ν_{107}	1306		0.05	$N2H_2$ twist., C16H bend., $C22H_3$ rock., **1**, $N31H_2$ twist., C45H bend., $C51H_3$ rock., **2**, iph.
ν_{106}	1293	1300	12	C=C str., as. Kekule, **2**
ν_{105}	1292	1300	12	C=C str., as. Kekule, **1**
ν_{104}	1268	1246	34	C_{Ar}–C str., **1**, **2**, ooph., CCH_{Ar} bend, CH bend.
ν_{103}	1266		0.3	C_{Ar}–C str., **1**, **2**, iph., CCH_{Ar} bend, CH bend.
ν_{102}	1264		3	CCH_{Ar} bend., **1**
ν_{101}	1264		2	CCH_{Ar} bend., **2**
ν_{100}	1221	1200	54	C_{Ar}–C str., CH bend., **1**, **2**, ooph.
ν_{99}	1216		0,00	C_{Ar}–C str., **1**, **2**, iph., CCH_{Ar} bend, CH bend.
ν_{98}	1191	1200	155	C_{Ar}–C str., CH bend., **1**, **2**, ooph.
ν_{97}	1187		0.3	C_{Ar}–C str., CH bend., **1**, **2**, iph.
ν_{96}	1175		14	CCH_{Ar} bend., C35–$C55H_{3\ Ar}$ str., **2**
ν_{95}	1175		3	CCH_{Ar} bend., C6–$C26H_{3\ Ar}$ str., **1**
ν_{94}	1148		1	CCH_{Ar} bend., **1**
ν_{93}	1148		1	CCH_{Ar} bend., **2**
ν_{92}	1139		3	$C22H_3$ rock., **1**, $C51H_3$ rock., **2**
ν_{91}	1137		0.00	$C22H_3$ rock., **1**, $C51H_3$ rock., **2**
ν_{90}	1117		2	CCH_{Ar} bend., **1**
ν_{89}	1116		2	CCH_{Ar} bend., **2**
ν_{88}	1094	1095	68	C22–N2 str., C16–N2 str., ooph., C16H bend., $C18H_3$ twist., $C22H_3$ twist., **1**
ν_{87}	1094		9	C51–N31 str., C45–N31 str., ooph., C45H bend., $C47H_3$ twist., $C51H_3$ twist., **2**
ν_{86}	1060		6	CCH_{Ar} bend., ring str., **2**
ν_{85}	1059		1	CCH_{Ar} bend., ring str., **2**
ν_{84}	1055		0.04	$N2H_2$ twist., C16–C18 str., **1**, $N31H_2$ twist., C45–C47 str., **2**, iph.
ν_{83}	1053		8	$N2H_2$ twist., C16–C18 str., **1**, $N31H_2$ twist., C45–C47 str., **2**, ooph.
ν_{82}	1049		0.8	$C26H_{3\ Ar}$ rock., **1**, $C55H_{3\ Ar}$ rock., **2**
ν_{81}	1048	1049	15	$C26H_{3\ Ar}$ rock., **1**, $C55H_{3\ Ar}$ rock., **2**
ν_{80}	1034	1030	14	N2–$C22H_3$ str., C16–$C18H_3$ str., iph., C16–N2 str., ooph., **1**
ν_{79}	1033	1030	9	N31–$C51H_3$ str., C45–$C47H_3$ str., iph., C45–N31 str., ooph., **2**
ν_{78}	1016		0.8	$C55H_{3\ Ar}$ rock., ring str., **2**
ν_{77}	1015		0.7	$C26H_{3Ar}$ rock., ring str., **1**
ν_{76}	1013	1007	43	C16–$C18H_3$ str., N2–$C22H_3$ str., ooph., **1**, C45–$C47H_3$ str., N31–$C51H_3$ str., ooph., **2**, **1** and **2**, ooph.
ν_{75}	1010		0.01	C16–$C18H_3$ str., **1**, C45–$C47H_3$ str., **2**
ν_{74}	988		0.06	CH_{Ar} oop. bend., ooph., **2**
ν_{73}	988		0.05	CH_{Ar} oop. bend., ooph., **1**
ν_{72}	976	973	38	$N2H_2$ rock., $C22H_3$ rock., **1**, $N31H_2$ rock., $C51H_3$ rock., **2**
ν_{71}	970	973	11	C16–C15 str., ring def., CH_3 rock., **1**, C44–C45 str., ring def., CH_3 rock., **2**, iph.
ν_{70}	970	973	143	C16–C15 str., ring def., CH_3 rock., $N2H_2$ rock., **1**, C44–C45 str., ring def., CH_3 rock., $N31H_2$ rock., **2**, ooph.
ν_{69}	950		0.004	$N2H_2$ rock., $C22H_3$ rock., **1**, $N31H_2$ rock., $C51H_3$ rock., **2**
ν_{68}	944	947	13	CH_{Ar} oop. bend., ooph., **2**
ν_{67}	944	947	8	CH_{Ar} oop. bend., ooph., **1**
ν_{66}	878		1	CH_{Ar} oop. bend., ooph., **2**
ν_{65}	877		1	CH_{Ar} oop. bend., ooph., **1**
ν_{64}	852		0.5	N2– C16 str., **1**, N31–C45 str., **2**, iph.
ν_{63}	852	845	11	N2– C16 str., **1**, N31–C45 str., **2**, ooph.
ν_{62}	801	798	11	Ring def., ip., as., $C6_{Ar}$–$C26H_3$ str., **1**
ν_{61}	800		3	Ring def., ip., as., $C35_{Ar}$–$C55H_3$ str., **2**
ν_{60}	789	781	6	CH_{Ar} oop. bend., iph., **2**
ν_{59}	788	781	11	CH_{Ar} oop. bend., iph., **1**
ν_{58}	755	752	40	CCH_{Ar} oop. bend., **1**, **2**
ν_{57}	755	752	6	CCH_{Ar} oop. bend., **1**, **2**

Mode	DFT freq. calc.	Exp. [29]	I_{IR}	Assignment
ν_{56}	732	728	16	CCH_{Ar} oop. bend., iph., **2**
ν_{55}	732	728	8	CCH_{Ar} oop. bend., iph., **1**
ν_{54}	677	671	11	CCH_{Ar} oop. bend., **2**
ν_{53}	675	671	13	CCH_{Ar} oop. bend., **1**
ν_{52}	641	636	7	Ring def., ip., as., C45N31C51 bend., **2**
ν_{51}	639	636	5	Ring def., ip., as., C16N2C22 bend., **1**
ν_{50}	568	564	3	Ring def., ip., as., C45N31C51 bend., **2**
ν_{49}	568		2	Ring def., ip., as., C16N2C22 bend., **1**
ν_{48}	526	524	12	CCH_{Ar} oop. bend., **2**
ν_{47}	525		1	CCH_{Ar} oop. bend., **1**, **2**
ν_{46}	480	478	3	CCH_{Ar} oop. bend., iph., **1**
ν_{45}	480	478	3	CCH_{Ar} oop. bend., iph., **2**

Abbreviations: DFT freq. calc.. – calculated frequency with scale factor, cm^{-1}; exp. – experimental; I_{IR} – calculated IR intensity, km/mol; Ar – aryle; def. – deformation; str. – bond stretching; rock. – rocking, twist. – twisting, wag. – wagging, bend. – bending, scis. – scissoring deformation vibrations; s. – symmetric and as. − asymmetric vibrations; ooph. – out-of-phase; iph. – in-phase; ip. – in-plane; oop. – out-of-plane.
The bold symbol denotes the number of molecules in dimer 1.

Table S4. Calculated frequencies, IR intensities, corresponding experimental date, and assignment of vibrational modes for the dimer 2 of 2-methylmethcathinone hydrochloride determined at the B3LYP/6-31G(d,p) level.

Mode	DFT freq. calc.	Exp. [29]	I_{IR}	Assignment
ν_{174}	3387	3372 [33]	59	N2–H4 str., **1**
ν_{173}	3379	3372 [33]	65	N31–H33 str., **2**
ν_{172}			3	$C22H_3$ str., as., **1**
ν_{171}			1	C–H_{Ar} str., iph., **1**, **2**, iph.
ν_{170}	3034	3024	34	C–H_{Ar} str., iph., **1**, **2**, ooph.
ν_{169}	3031		3	$C51H_3$ str., as., **2**
ν_{168}	3018		14	C–H_{Ar} str., ooph., **1**
ν_{167}	3018		14	C–H_{Ar} str., ooph., **2**
ν_{166}	3017		2	$C22H_3$ str., as., **1**
ν_{165}	3016		2	$C51H_3$ str., as., **2**
ν_{164}	3003		11	C–H_{Ar} str., ooph., **1**
ν_{163}	3002		12	C–H_{Ar} str., ooph., **2**
ν_{162}	2997		4	$C47H_3$ str., as., **2**
ν_{161}	2993		4	$C18H_3$ str., as., **1**
ν_{160}	2985	2984	132	$C42_{Ar}$–H43 str. (**2**)···Cl 60 (**1**)
ν_{159}	2984	2984	92	$C13_{Ar}$–H14 str. (**1**)···Cl 59 (**2**)
ν_{158}	2964	2959	7	$C47H_3$ str., as., **2**
ν_{157}	2963	2959	8	$C18H_3$ str., as., **1**
ν_{156}	2962	2959	15	$C55H_{3\,Ar}$ str., as., **2**
ν_{155}	2962	2959	17	$C26H_{3\,Ar}$ str., as., **1**
ν_{154}	2947	2959	17	$C55H_{3\,Ar}$ str., as., **2**
ν_{153}	2946	2959	18	$C26H_{3\,Ar}$ str., as., **1**
ν_{152}	2933	2920	6	$C22H_3$ str., s., **1**
ν_{151}	2932	2920	6	$C51H_3$ str., s., **2**
ν_{150}	2895	2895	8	$C47H_3$ str., s., **2**
ν_{149}	2894	2895	8	$C18H_3$ str., s., **1**
ν_{148}	2887	2895	21	$C55H_{3\,Ar}$ str., s., **2**
ν_{147}	2887	2895	21	$C26H_{3\,Ar}$ str., s., **1**
ν_{146}	2878	2895	158	C45–H str., (**2**)···Cl 60 (**1**)
ν_{145}	2876	2895	83	C16–H str., (**1**)···Cl 59 (**2**)
ν_{144}	2451	2451	749	N2–H3–Cl 60 str., **1**, N31–H32–Cl 59 str., **2**, ooph.
ν_{143}	2364	2361	109	N2–H3–Cl 60 str., **1**, N31–H32–Cl 59 str., **2**, iph.
ν_{142}	1691	1696	224	C=O str., NH_2 scis., **1**, **2**, ooph.
ν_{141}	1691	1696	92	C=O str., NH_2 scis., **1**, **2**, iph.
ν_{140}	1606	1600	18	C35=C36 and C40=C42 str., s., **2**
ν_{139}	1606	1600	19	C6=C7 and C11=C13 str., s., **1**
ν_{138}	1574	1572	3	NH_2 scis., **1**
ν_{137}	1574	1572	42	NH_2 scis., **2**.

Mode	DFT freq. calc.	Exp. [29]	I_{IR}	Assignment
ν_{136}	1536	1550	85	C5=C6 and C9=C11 str., s., **1**, C34=C35 and C38=C40 str., s., **2**, iph.
ν_{135}	1536	1550	38	C5=C6 and C9=C11 str., s., **1**, C34=C35 and C38=C40 str., s., **2**, ooph.
ν_{134}	1488	1489	31	C=C str., as., **2**
ν_{133}	1487	1489	30	C=C str., as., **1**
ν_{132}	1463	1459	43	$C18H_3$ def., as., $C22H_3$ def., as., $N2H_2$ wag., **1**, $C47H_3$ def., as., $C51H_3$ def., as., $N31H_2$ wag., **2**, ooph.
ν_{131}	1462	1459	2	$C18H_3$ def., as., $C22H_3$ def., as., $N2H_2$ wag., **1**, $C47H_3$ def., as., $C51H_3$ def., as., $N31H_2$ wag., **2**, iph.
ν_{130}	1459	1459	32	$C18H_3$ def., as., $C22H_3$ def., as., $N2H_2$ wag., **1**, $C47H_3$ def., as., $C51H_3$ def., as., $N31H_2$ wag., **2**, ooph.
ν_{129}	1458	1459	25	$C18H_3$ def., as., $C22H_3$ def., as., $N2H_2$ wag., **1**, $C47H_3$ def., as., $C51H_3$ def., as., $N31H_2$ wag., **2**, iph.
ν_{128}	1452	1459	27	$C18H_3$ def., as., $C22H_3$ def., as., $N2H_2$ wag., **1**, $C47H_3$ def., as., $C51H_3$ def., as., $N31H_2$ wag., **2**, iph.
ν_{127}	1452	1459	88	$C18H_3$ def., as., $C22H_3$ def., as., $N2H_2$ wag., **1**, $C47H_3$ def., as., $C51H_3$ def., as., $N31H_2$ wag., **2**, ooph.
ν_{126}	1449	1459	31	$C26H_3$ def., as., **1**, $C55H_3$ def., as., **2**, ooph.
ν_{125}	1448	1459	8	$C26H_3$ def., as., **1**, $C55H_3$ def., as., **2**, iph.
ν_{124}	1445	1459	27	$C18H_3$ def., as., $C22H_3$ def., as., $N2H_2$ wag., **1**, $C47H_3$ def., as., $C51H_3$ def., as., $N31H_2$ wag., **2**, ooph.
ν_{123}	1445	1459	5	$C18H_3$ def., as., $C22H_3$ def., as., $N2H_2$ wag., **1**, $C47H_3$ def., as., $C51H_3$ def., as., $N31H_2$ wag., **2**, iph.
ν_{122}	1436		14	$C26H_3$ def., as.,**1**, $C55H_3$ def., as., **2**, ooph.
ν_{121}	1436		2	$C26H_3$ def., as.,**1**, $C55H_3$ def., as., **2**, iph.
ν_{120}	1430	1430	47	$C18H_3$ def., as., $C22H_3$ def., as., $N2H_2$ wag., **1**, $C47H_3$ def., as., $C51H_3$ def., as., $N31H_2$ wag., **2**, ooph.
ν_{119}	1428	1430	3	$C18H_3$ def., as., $C22H_3$ def., as., $N2H_2$ wag., **1**, $C47H_3$ def., as., $C51H_3$ def., as., $N31H_2$ wag., **2**, iph.
ν_{118}	1419	1417	1	C=C str., as., $C26H_{3\,Ar}$ def., as., **1**
ν_{117}	1419	1417	1	C=C str., as., $C55H_{3\,Ar}$ def., as., **2**
ν_{116}	1400		14	$C51H_3$ def., s., $N31H_2$ twist., **2**
ν_{115}	1396		18	$C22H_3$ def., s., $N2H_2$ twist., **1**
ν_{114}	1388	1380	55	$C51H_3$ def., s., $N31H_2$ twist., **2**
ν_{113}	1388	1380	16	$C22H_3$ def., s., $N2H_2$ twist., **1**
ν_{112}	1374		1	$C55H_3$ def., s., **2**
ν_{111}	1374		10	$C47H_3$ def., s.,$C55H_{3\,Ar}$ def., s., $N31H_2$ wag., C45H bend., **2**
ν_{110}	1373		5	$C18H_3$ def., s., $C26H_{3\,Ar}$ def., s., $N2H_2$ wag., C16H bend., **1**
ν_{109}	1372		18	$C18H_3$ def., s., $C26H_{3\,Ar}$ def., s., $N2H_2$ wag., C16H bend., **1**
ν_{108}	1340		1	C16H bend., $N2H_2$ twist., $C22H_3$ rock., **1**, C45H bend., $N31H_2$ twist., $C51H_3$ rock., **2**, iph.
ν_{107}	1336	1336	15	C16H bend., $N2H_2$ twist., $C22H_3$ rock., **1**, C45H bend., $N31H_2$ twist., $C51H_3$ rock., **2**, ooph.
ν_{106}	1296		2	C16H bend., **1**
ν_{105}	1294	1300	8	C45H bend., **2**
ν_{104}	1294	1300	17	C=C str., as. Kekule, **2**
ν_{103}	1293	1300	13	C=C str., as. Kekule, **1**
ν_{102}	1276		1	CCH_{Ar} bend., **2**
ν_{101}	1276		1	CCH_{Ar} bend., **1**
ν_{100}	1220	1200	70	C_{Ar}–C str., CH bend., **1**, **2**, iph.
ν_{99}	1220	1200	123	C_{Ar}–C str., CH bend., **1**, **2**, ooph.
ν_{98}	1182		3	C35–$C55H_{3\,Ar}$ str., **2**
ν_{97}	1181		2	C6–$C26H_{3\,Ar}$ str. **1**
ν_{96}	1174	1166	7	$C22H_3$ rock., $C18H_3$ rock., $N2H_2$ rock., **1**
ν_{95}	1174	1166	18	$C51H_3$ rock., $C47H_3$ rock., $N31H_2$ rock., **2**
ν_{94}	1149		2	CCH_{Ar} bend., **1**, **2**, ooph.
ν_{93}	1149		0	CCH_{Ar} bend., **1**, **2**, iph.
ν_{92}	1136		2	$C22H_3$ rock., $N2H_2$ rock., C16H bend., CCH_{Ar} bend., **1**, $C51H_3$ rock., $N31H_2$ rock., C45H bend., CCH_{Ar} bend., **2**, iph.
ν_{91}	1136	1137	29	$C22H_3$ rock., $N2H_2$ rock., C16H bend., CCH_{Ar} bend., **1**, $C51H_3$ rock., $N31H_2$ rock., C45H bend., CCH_{Ar} bend., **2**, ooph.
ν_{90}	1125	1137	49	$C22H_3$ rock., $N2H_2$ rock., C16H bend., **1**, $C51H_3$ rock., $N31H_2$ rock., C45H bend., **2**, CCH_{Ar} bend., **1**, **2**, ooph.
ν_{89}	1123		3	$C22H_3$ rock., $N2H_2$ rock., C16H bend., **1**, $C51H_3$ rock., $N31H_2$ rock., C45H bend., **2**, CCH_{Ar} bend., **1**, **2**, iph.

Mode	DFT freq. calc.	Exp. [29]	I_{IR}	Assignment
ν_{88}	1101	1095	124	C22–N2 str., C16–N2 str., ooph., C16H bend., $C18H_3$ twist., $C22H_3$ twist., **1**, C51–N31 str., C45–N31 str., ooph., C45H bend., $C47H_3$ twist., $C51H_3$ twist., **2**, ooph.
ν_{87}	1099		0	C22–N2 str., C16–N2 str., ooph., C16H bend., $C18H_3$ twist., $C22H_3$ twist., **1**, C51–N31 str., C45–N31 str., ooph., C45H bend., $C47H_3$ twist., $C51H_3$ twist., **2**, iph.
ν_{86}	1054	1049	13	$C47H_3$ rock., $C51H_3$ rock., **2**
ν_{85}	1054	1049	15	$C18H_3$ rock., $C22H_3$ rock., **1**
ν_{84}	1050		1	Ring str., **2**
ν_{83}	1050		0	Ring str. **1**
ν_{82}	1042		7	$C55H_{3\,Ar}$ rock., **2**
ν_{81}	1042		6	$C26H_{3\,Ar}$ rock., **1**
ν_{80}	1031		1	N2–C16 str., N2–$C22H_3$ str., C16–$C18H_3$ str., **1**, N31–C45 str., N31–$C51H_3$ str., C45–$C47H_3$ str., **2**, iph.
ν_{79}	1031	1030	26	N2–C16 str., N2–$C22H_3$ str., C16–$C18H_3$ str., **1**, N31–C45 str., N31–$C51H_3$ str., C45–$C47H_3$ str., **2**, ooph.
ν_{78}	1005	1007	7	N31–$C51H_3$ str., C45–N31 str., ooph., CCH_{Ar} oop. bend., **2**
ν_{77}	1002	1007	8	N2–$C22H_3$ str., C16–N2 str., ooph., CCH_{Ar} oop. bend., **1**
ν_{76}	986		1	$C55H_{3\,Ar}$ rock., **2**
ν_{75}	986		0	$C26H_{3\,Ar}$ rock., **1**
ν_{74}	971	973	30	C44–C45 str., CH_{Ar} oop. bend., CH_3 rock., **2**
ν_{73}	969	973	7	C15–C16 str., CH_{Ar} oop. bend., CH_3 rock., **1**
ν_{72}	958		5	N31–$C51H_3$ str., CH_{Ar} oop. bend., ooph., **2**
ν_{71}	957		3	N2–$C22H_3$ str., CH_{Ar} oop. bend., ooph., **1**
ν_{70}	943	947	18	C44–C45 str., CH_{Ar} oop. bend., $C47H_3$ rock., **2**
ν_{69}	942	947	137	C15–C16 str., CH_{Ar} oop. bend., $C18H_3$ rock., **1**
ν_{68}	875		1	CH_{Ar} oop. bend., ooph., **2**
ν_{67}	874		1	CH_{Ar} oop. bend., ooph., **1**
ν_{66}	850	845	30	C–N str., **2**
ν_{65}	850	845	26	C–N str., **1**
ν_{64}	812		4	$N2H_2$ rock., $C22H_3$ rock., $C18H_3$ rock., **1**
ν_{63}	811		3	$N31H_2$ rock., $C51H_3$ rock., $C47H_3$ rock., **2**
ν_{62}	786		4	CCH_{Ar} iph. oop. bend., **1**, **2**, ooph.
ν_{61}	786	781	28	CCH_{Ar} oop. bend., **1**
ν_{60}	782		2	Ring def., ip., as., $C35_{Ar}$–$C55H_3$ str., **2**
ν_{59}	782		7	Ring def., ip., as., $C6_{Ar}$–$C26H_3$ str., **1**
ν_{58}	755	752	47	CCH_{Ar} iph., oop. bend., **1**, **2**, ooph.
ν_{57}	755	752	0	CCH_{Ar} iph., oop. bend., **1**, **2**, iph.
ν_{56}	726	728	12	CCH_{Ar} oop. bend., **1**, **2**, ooph.
ν_{55}	725	728	4	CCH_{Ar} oop. bend., **1**, **2**, iph.
ν_{54}	671	671	11	CCH_{Ar} oop. bend., **1**
ν_{53}	671	671	2	CCH_{Ar} oop. bend., **2**
ν_{52}	634	636	1	Ring def., ip., **2**,
ν_{51}	631	636	1	Ring def., ip., **1**
ν_{50}	560	564	2	Ring def., ip., **1**
ν_{49}	560	564	6	Ring def., ip., **2**
ν_{48}	527	524	25	CCH_{Ar} oop. bend., ooph., **2**
ν_{47}	525	524	4	CCH_{Ar} oop. bend., ooph., **1**
ν_{46}	477	478	7	CCH_{Ar} oop. bend., ooph., **2**
ν_{45}	476	478	3	CCH_{Ar} oop. bend., ooph., **1**

Abbreviations: DFT freq. calc.. – calculated frequency with scale factor, cm^{-1}; exp. – experimental; I_{IR} – calculated IR intensity, km/mol; Ar – aryle; def. – deformation; str. – bond stretching; rock. – rocking, twist. – twisting, wag. – wagging, bend. – bending, scis. – scissoring deformation vibrations; s. – symmetric and as. – asymmetric vibrations; ooph. – out-of-phase; iph. – in-phase; ip. – in-plane; oop. – out-of-plane.
Bold symbol denotes the number of molecule in the dimer 2.

Table S5. Calculated frequencies, IR intensities, corresponding experimental date and assignment of vibrational modes for the dimer of 4-methylmethcathinone hydrochloride determined at the B3LYP/6-31G(d,p) level

Mode	DFT freq. calc.	Exp. [29]	I_{IR}	Assignment
ν_{174}	3358	3356 [32]	40	N3–H5 str., **1**
ν_{173}	3092		2	C–H_{Ar} str., iph., **2**
ν_{172}	3088		4	C–H_{Ar} str., iph., **1**
ν_{171}	3078	3065	13	C–H_{Ar} str., iph., **2**

Mode	DFT freq. calc.	Exp. [29]	I_{IR}	Assignment
ν_{170}	3066		1	$C42H_3$ str., as., **2**
ν_{169}	3065	3065	11	C–H_{Ar} str., iph., **1**
ν_{168}	2999	3000	13	C–H_{Ar} str., ooph., **2**
ν_{167}	2997	3000	18	C–H_{Ar} str., ooph., $C13H_3$ str., as., **1**
ν_{166}	2996	3000	18	C–H_{Ar} str., ooph., $C13H_3$ str., as., **1**
ν_{165}	2995	3000	12	C–H_{Ar} str., ooph., **2**
ν_{164}	2995	3000	8	$C42H_3$ str., as., **2**
ν_{163}	2994	3000	14	C–H_{Ar} str., ooph., **1**
ν_{162}	2989	3000	7	$C13H_3$ str., as., **1**
ν_{161}	2970	2967	11	$C18H_3$ str., as., **1**
ν_{160}	2966	2967	15	$C47H_3$ str., as., **2**
ν_{159}	2961	2967	9	$C47H_3$ str., as., **2**
ν_{158}	2951	2942	5	$C18H_3$ str., as., **1**
ν_{157}	2950	2942	14	$C55H_{3\,Ar}$ str., as., **2**
ν_{156}	2946	2942	16	$C26H_{3\,Ar}$ str., as., **1**
ν_{155}	2920	2917	14	$C55H_{3\,Ar}$ str., as., **2**
ν_{154}	2917	2917	19	$C26H_{3\,Ar}$ str., as., **1**
ν_{153}	2914	2904	25	$C42H_3$ str., s., C35–H36 str., **2**
ν_{152}	2909	2904	12	$C42H_3$ str., s., C35–H36 str., **2**
ν_{151}	2878	2871	41	$C13H_3$ str., s., C6–H7 str., **1**
ν_{150}	2866	2871	10	$C47H_3$ str., s., **2**, C6–H7 str., **1**
ν_{149}	2756	2740	121	N32–H34 (**2**)···Cl 1 (**1**) str.
ν_{148}	2743	2740	184	N32–H34 (**2**)···Cl 1 (**1**) str.
ν_{147}	2738		18	$C55H_{3\,Ar}$ str., s., **2**
ν_{146}	2734	2740	165	N32–H34 (**2**)···Cl 1 (**1**) str.
ν_{145}	2734	2740	389	N32–H34 (**2**)···Cl 1 (**1**) str.
ν_{144}	2458	2451	805	N3–H4–Cl 1 str., **1**, N32–H33–Cl 2 str., **2**, ooph.
ν_{143}	2410	2418	131	N3–H4–Cl 1 str., **1**, N32–H33–Cl 2 str., **2**, iph.
ν_{142}	1716	1684	161	C=O str., $N32H_2$ scis., **2**
ν_{141}	1689	1684	190	C=O str., $N3H_2$, scis., **1**
ν_{140}	1606	1605	72	C53=C59 and C40=C51 str., s., **2**
ν_{139}	1606	1605	107	C24=C30 and C11=C22 str., s., **1**
ν_{138}	1578	1569	34	$N32H_2$ scis., **2**
ν_{137}	1562	1569	10	C39=C40 and C59=C46 str., s., **2**
ν_{136}	1562	1569	11	C10=C11 and C30=C17 str., s., **1**
ν_{135}	1542	1569	95	$N3H_2$ scis., **1**
ν_{134}	1502	1492	2	C=C str., as., **1**
ν_{133}	1497	1492	1	C=C str., as., **2**
ν_{132}	1485	1467	85	$C42H_3$ def., as., $N32H_2$ wag., **2**
ν_{131}	1474	1467	25	$C13H_3$ def., as., $N3H_2$ wag., **1**
ν_{130}	1472	1467	28	$C42H_3$ def., as., $C47H_3$ def., as., **2**
ν_{129}	1472	1467	5	$C13H_3$ def., as., $C18H_3$ def., as., **1**
ν_{128}	1461	1457	12	$C47H_3$ def., as., **2**
ν_{127}	1458	1457	3	$C13H_3$ def., as., $C18H_3$ def., as., **1**, $C42H_3$ def., as., $C47H_3$ def., as., $N32H_2$ twist., **2**
ν_{126}	1457	1457	31	$C42H_3$ def., as., $C47H_3$ def., as., $N32H_2$ twist., **2**, $C13H_3$ def., as., $C18H_3$ def., as., $N3H_2$ twist., **1**
ν_{125}	1453	1457	2	$C13H_3$ def., as., $C18H_3$ def., as., $N3H_2$ wag., C6H7 bend, **1**
ν_{124}	1453	1457	9	$C55H_{3\,Ar.}$ def., as., **2**
ν_{123}	1452	1457	10	$C26H_3$ def., as., **1**
ν_{122}	1449	1457	14	$C13H_3$ def., as., $C18H_3$ def., as., $N3H_2$ twist., C6H7 bend, **1**
ν_{121}	1448	1457	5	$C26H_3$ def., as., **1**
ν_{120}	1446	1457	6	$C55H_3$ def., as., **2**
ν_{119}	1437	1457	8	$C42H_3$ def., as., $N3H_2$ wag., **2**
ν_{118}	1423	1412	18	$C13H_3$ def., s., $C18H_3$ def., s., $N3H_2$ wag., C6H7 bend., **1**
ν_{117}	1412	1412	6	$C13H_3$ def., s., $C18H_3$ def., s., $N3H_2$ twist., C6H7 bend., **1**
ν_{116}	1407	1412	5	$C42H_3$ def., s., **2**
ν_{115}	1400	1412	13	C53=C59 and C40=C51 str., as., $N32H_2$ twist., C35H36 bend., **2**
ν_{114}	1398	1412	21	C24=C30 and C11=C22 str., as., $N3H_2$ twist., C6H7 bend., **1**
ν_{113}	1382	1384	83	$C47H_3$ def., s., $N32H_2$ twist., C35H36 bend., **2**
ν_{112}	1377		2	$C55H_3$ def., s., **2**
ν_{111}	1376	1384	22	$C47H_3$ def., s., $N32H_2$ twist., **2**
ν_{110}	1374		1	$C26H_3$ def., s., **1**
ν_{109}	1373		7	$C18H_3$ def., s., **1**
ν_{108}	1330	1347	42	$N32H_2$ twist., C35H bend, **2**

Mode	DFT freq. calc.	Exp. [29]	I_{IR}	Assignment
ν_{107}	1310	1295	9	C=C str., as. Kekule, **1**
ν_{106}	1310	1295	1	C=C str., as. Kekule, **2**
ν_{105}	1308	1295	94	Ring str., C6–C8 str., C6H7 bend., $N3H_2$ twist., **1**
ν_{104}	1299	1295	25	Ring str., C6–C8 str., C6H7 bend., $N3H_2$ twist., **1**
ν_{103}	1294	1295	7	Ring str., C35H bend., **1**
ν_{102}	1288	1295	15	C6H7 bend., C6–C8 str., C8–$C10_{Ar}$ str., ooph., $N3H_2$ twist., **1**
ν_{101}	1280	1295	43	C35H36 bend., C35–C37 str., C37–$C39_{Ar}$ str., ooph., **2**
ν_{100}	1256	1248	107	C8–$C10_{Ar}$ str., C6–N3 str., C6H bend., **1**
ν_{99}	1236	1248	121	C37–$C39_{Ar}$ str., C35–N32 str., C35H bend., **2**
ν_{98}	1214		1	$C26H_3$–$C17_{Ar}$ str., CCH_{Ar} bend., **1**
ν_{97}	1213	1215	17	$C55H_3$–$C46_{Ar}$ str., CCH_{Ar} bend., **2**
ν_{96}	1201		1	CCH_{Ar} bend., $N3H_2$ rock., **1**
ν_{95}	1196	1201	20	CCH_{Ar} bend., $N32H_2$ rock., **2**, CCH_{Ar} bend., **1**
ν_{94}	1194	1201	13	CCH_{Ar} bend., NH_2 rock., **1**, **2**
ν_{93}	1186	1189	34	CCH_{Ar} bend., $N32H_2$ rock., **2**
ν_{92}	1164	1166	5	C6–N3 str., C6H7 bend., $C13H_3$ rock., **1**
ν_{91}	1160	1166	7	C35–N32 str., C35H36 bend., $C42H_3$ rock., **2**
ν_{90}	1128	1126	13	CCH_{Ar} bend., **1**
ν_{89}	1126	1126	12	CCH_{Ar} bend., **2**
ν_{88}	1098	1096	50	C35–N32 str., N32–$C42H_3$ str., ooph., $C47H_3$, $C42H_3$ rock., **2**
ν_{87}	1097	1096	25	C6–N3 str., N3–$C13H_3$ str., ooph., $C13H_3$, $C18H_3$ rock., **1**
ν_{86}	1058		8	N32–$C42H_3$ str., C35–$C47H_3$ str., $N32H_2$ twist., **2**
ν_{85}	1055		6	N3–$C13H_3$ str., C6–$C18H_3$ str., $N3H_2$ twist., **1**
ν_{84}	1054	1050	5	$C55H_3$ rock., **2**
ν_{83}	1052	1050	13	$C26H_3$ rock., **1**
ν_{82}	1048	1050	13	C35–N3 str., N32–$C42H_3$ str., ooph., C35– $C47H_3$ str., **2**
ν_{81}	1035	1030	15	C6–N3 str., N3–$C13H_3$ str., ooph., C6– $C18H_3$ str., **1**
ν_{80}	1029		2	Ring def., as., **1**
ν_{79}	1028		1	Ring def., as., **2**
ν_{78}	1013	1008	21	N32–$C42H_3$ str., $C47H_3$ rock., $C55H_3$ rock., **2**
ν_{77}	1008	1008	14	N3–$C13H_3$ str., $C18H_3$ rock., $C26H_3$ rock., **1**
ν_{76}	1006	1008	40	$C55H_3$ rock., N32–$C42H_3$ str., **2**
ν_{75}	1005		8	$C26H_3$ rock., N3–$C13H_3$ str., **1**
ν_{74}	990 sh.	976	6	CH_{Ar} oop. bend., ooph., **1**, **2**
ν_{73}	988 sh.	976	17	CH_{Ar} oop. bend., ooph., **1**, **2**
ν_{72}	982		2	CH_{Ar} oop. bend., ooph., **1**
ν_{71}	978	976	42	CH_{Ar} oop. bend., ooph., C6–C8 str., N3–$C13H_3$ str., iph., $C18H_3$ rock., **1**
ν_{70}	973	976	48	CH_{Ar} oop. bend., ooph., C35–C37 str., N32–$C42H_3$ str., iph., $C47H_3$ rock., **2**
ν_{69}	946		4	CH_{Ar} oop. bend., ooph., **2**
ν_{68}	912	889	35	$N32H_2$, rock., **2**
ν_{67}	863	889	41	$N3H_2$, rock., **1**
ν_{66}	851	854	4	CH_{Ar} oop. bend., ooph., **1**, **2**
ν_{65}	848	854	6	CH_{Ar} oop. bend., ooph., **1**, **2**
ν_{64}	841	854	4	N32–C35 str., ring breathing, **2**
ν_{63}	836	844	20	CH_{Ar} oop. bend., iph., **1**
ν_{62}	824	828	12	CH_{Ar} oop. bend., iph., **2**
ν_{61}	822	828	16	N3–C6 str., ring breathing, **1**
ν_{60}	802	802	5	$C46_{Ar}$–$C55H_3$ str., ring str., s., **2**
ν_{59}	801	802	8	$C17_{Ar}$–$C26H_3$ str., ring str., s., **1**
ν_{58}	753	757	18	CCH_{Ar} oop. bend., iph., **1**
ν_{57}	746	757	9	CCH_{Ar} oop. bend., iph., **2**
ν_{56}	735	733	10	CCH_{Ar} oop. bend., iph., **1**
ν_{55}	731	733	8	CCH_{Ar} oop. bend., iph., **2**
ν_{54}	688	687	6	Ring def., oop, **1**
ν_{53}	682	687	4	Ring def., oop, **2**
ν_{52}	639		1	Ring def., ip., as., **2**
ν_{51}	638		0.1	Ring def., ip., as., **1**
ν_{50}	599	600	7	Ring def., ip., s., **1**
ν_{49}	598	600	3	Ring def., ip., s., **2**
ν_{48}	512	510	5	$N3H_2^+$ libration movement relative Cl 1 atom, **1**
ν_{47}	507	510	18	$N32H_2^+$ libration movement relative Cl 2 atom, **2**
ν_{46}	480	478	8	CCH_{Ar} oop. bend., iph., **1**
ν_{45}	480	478	18	CCH_{Ar} oop. bend., iph., **2**

Abbreviations: DFT freq. calc.. – calculated frequency with scale factor, cm^{-1}; exp. – experimental; I_{IR} – calculated IR intensity, km/mol; Ar – aryle; def. – deformation; str. – bond stretching; rock. – rocking, twist. – twisting, wag. – wagging, bend. – bending, scis. – scissoring deformation vibrations; s. – symmetric and as. − asymmetric vibrations; ooph. – out-of-phase; iph. – in-phase; ip. – in-plane; oop. – out-of-plane.
Bold symbol denotes the number of molecules in the dimer.

SM:

The aromatic in-plane CCH deformation vibrations (CCH_{Ar} bend) are predicted in 1276–1060 cm^{-1} (Tables S3–S5) with a very weak IR absorption. In the IR spectrum of the 4-MMC dimer, this type of vibration forms the independent weak experimental band 1126 cm^{-1} (calc.: 1128 and 1126 cm^{-1}) and provides contributions to experimentally observed IR absorption at 1189 cm^{-1} (Figure 8 in the main text). The rest of the CCH_{Ar} bend. Vibrations do not give visible bands due to weak IR absorption. The out-of-plane deformation vibrations CCH produce experimental IR bands 1007, 973, 947, 781, 752, 728, 671, 524, 478 cm^{-1} in the spectrum of 2-MMC compound (Figure 7) and 976, 854, 844, 828, 757, 733, 478 cm^{-1} in the spectrum of 4-MMC compound (Figure 8); however, the calculated absorption intensities are, as a rule, lower than the experimental ones.